

Award Accounts

The Chemical Society of Japan Award for Young Chemists for 2008

Molecular Theory Including Quantum Effects and Thermal Fluctuations

Yasuteru Shigeta

Picobiology Institute, Graduate School of Life Science, University of Hyogo,
3-2-1 Koto, Kamigori-cho, Ako-gun, Hyogo 678-1297

Core Research for Evolutional Science and Technology, Japan Science and Technology Agency (CREST, JST),
Chiyoda-ku, Tokyo 102-0075

Received July 31, 2009; E-mail: shigeta@sci.u-hyogo.ac.jp

Recent progress in our theoretical developments and applications where thermal fluctuations and quantum effects are important are reviewed. We first show that motions of a confined atom coupled with a fullerene cage cause large thermal fluctuation of the effective charge on the confined atom and that the fluctuation is sensitive to applied temperature and the number of confined species. Second, two different approaches to treat nuclear quantum effects are discussed. One is non-Born–Oppenheimer (NBO) molecular theory, which is one of an extension of molecular orbital theory for electrons to nuclear motions. This method is suitable to describe static and stationary nuclear (vibrational) states so we apply this method to obtain vibrationally coupled electron density of a protonatable amino acid. We compare the obtained electron density through NBO treatment with conventional calculations. The other approach is referred as to quantum cumulant dynamics (QCD), which is a generalization of quantized Hamiltonian dynamics initially proposed by Prezhdo. This method is applied to vibrational analyses. The ordinary normal mode analysis (NMA) is extended to include quantum degrees of freedom based on QCD formalism, which gives a better description of the vibrational state, where ordinary NMA gives incorrect results. Vibrational frequencies of small molecules by the QCD simulation are compared with those by classical molecular dynamics (MD). It is found that QCD is superior to classical MD in that the results obtained by QCD are in good agreement with those by full quantum treatment. Finally the theoretical background of a real-space grid-based time-dependent density functional theory (RSTDDFT) is explained. This method is applied to solve a NBO problem by using an imaginary time propagator and electron dynamics driven by an off-resonant circularly polarized laser plus in addition to using a real time propagator. For the latter case, we investigate atom-centered dipole moment and induced current and detect the electronic fluctuation in a SiH_4 molecule after irradiation.

1. Introduction

There are many uncertain and mysterious problems observed around us in life. For example, ever-changing shapes of clouds and diffusion pattern of milk in coffee, are typical observations. Chemists and physicists have sought underlying mechanisms and apply models to simulate this evolution. Nevertheless we cannot often predict the future of the evolution even if we adopt the same conditions. In these cases, stochastic processes, fluctuations both in time and space, and nonlinear response play important roles.[1] Recently, the concept of fluctuations has become more important in many fields of physics, chemistry, and biology. In particular, some proteins undergo free energy induced structural change before proceeding to chemical reaction, where fluctuation is a necessary factor.

Thermodynamics has shown that homogeneous macroscopic systems exhibit certain universal properties without fluctuation.[2] Strictly speaking, the systems have historically been observed to exhibit explicit fluctuations, but they were out of experimental accuracy. Later, statistical mechanics were established to describe the nature of the fluctuations accompanied by thermodynamics mean (or averaged) values and relationships among them at a microscopic level.[3] In the beginning, the fluctuations were thought to be very small. With innovations in nano- and mesoscopic technologies, one can observe many phenomena at nanometer size and less than millisecond scale with high accuracy. In these resolutions, the fluctuations sometimes become strongly influence the mean value.

At low temperature, quantum effects, which should be distinguished from the thermal fluctuation described above, exhibits a wide variety of fascinating phenomena at microscopic level, for instance, quantum interference, quantum tunneling, and zero-point vibration effects.[4] Discovery of quantum mechanics is one of the most important developments in the past century. Quantum mechanics can describe the microscopic properties of atoms, molecules, and condensed phases, which are fundamental topics in physical chemistry. Even for macroscopic phenomena, metal–insulator and metal–superconducting transitions, magnetism, and Bose–Einstein condensation are described by quantum mechanics with the

Published on the web November 10, 2009; doi:10.1246/bcsj.82.1323

help of statistical mechanics.[5,6] Quantum effects, such as zero point energy and tunneling are particularly essential, and cannot be avoided especially in molecular sciences. For example, to characterize reactions in chemically interesting systems, it is essential to take into consideration both dynamic fluctuation and quantum effects. Nevertheless, the many-body dynamics of these chemical reactions are too complicated and demanding to be simulated using full quantum dynamics methods. Therefore, full quantum dynamics methods are limited to a few degrees of freedom; i.e., to small systems.

In order to deal with thermal fluctuations and quantum effects, there are numerous methods describing them. Classical molecular dynamics (MD) simulation is good at treating thermal properties of systems,[7] since it can be used to perform long-time simulations owing to use of an approximate force field to describe bonded and non-bonded interactions. Ab initio first principle MD is also a useful method, which gives averaged values and fluctuations of both structural information and electronic structure simultaneously. Nevertheless these methods cannot treat the quantum nature of nuclear motions, such as vibration and quantum tunneling.

There are a number of approaches that can be used to treat these quantum effects, at least approximately.[8–21] The Schrödinger equation is solved to investigate quantum effects often by introducing basis sets. As an alternative, Feynman's path integral-based[16] and semiclassical,[9] such as the WKB approximation, methods are sometimes adopted to treat quantum tunneling. Path integrals are one of the easiest ways to incorporate quantum effects into classical dynamics. In the path integral method, the quantum effects are described by means of a summation of possible classical paths. Although an implementation of path integral MD into ordinary classical MD is quite easy, it is difficult to perform real-time quantum dynamics due to complicated analytic continuation. Therefore, the treatment of the quantum effects is more difficult than that of thermal effects.

In order to treat the quantum effects we have developed two different ways. One is a wave function based method, known as non-Born–Oppenheimer (NBO) molecular theory extensively studied recently,[22–56] and the other is cumulant based, called quantal cumulant dynamics (QCD).[57–68] The former is suitable to deal with stationary states of the nuclear motions and the latter with dynamic and non-stationary states.

The quantum nature of electrons is more remarkable than that of nuclei. In quantum chemistry, electrons are often treated as being static ones. But recent progress in attosecond laser technology has opened new possibilities, such as laser imaging, detection, and control of electrons directly. For this, we have developed a way to control electron ring-current in ring-shaped molecules by means of a circularly polarized laser pulse.[69] Recently we have implemented a real-time electron dynamics method by means of a grid basis.

In this review we discuss the following three topics: (1) The importance of thermal fluctuation in the molecular properties.[70–72] (2) Development of novel methods to treat nuclear quantum effects.[22–24,62–68] (3) Field driven electron dynamics in SiH_4 by means of real-time electron dynamics. Finally we conclude and give future perspectives of the fields.

2. Confinement and Fluctuation in a Molecular Cage: Endohedral Fullerene as a Typical Case

It is well known that the fullerene cages have two different three-dimensional (3D) reaction fields, namely, endohedral and exohedral. Exohedral fullerenes have been extensively studied for the last decade in many aspects ranging from catalytic chemistry to medically oriented nanotechnology.[73] Soon after the establishment of a systematic method to prepare fullerenes abundantly,[74] La@C_{84} was synthesized as the first endohedral fullerene.[75] Since then many studies have been dedicated to various endohedral fullerenes featuring, for instance, identification of the stable position of a La atom in C_{84} fullerene, synchronous rotation of two La atoms in C_{80}[76] injection of rare-gas atoms into the cage,[77] and discovery of unusual electron charge on an encapsulated N atom.[78] As for the dynamics inside the cage, it is now known that the motion of La in C_{82} is effectively frozen at temperature below 100 K, the gyration of induced dipole has been observed at 200 K, and the gyration axis fluctuates over 400 K[79] where the electronic structure of La is almost stable during the dynamics. Thus it is anticipated that the coupled dynamics of the cage and encapsulated compounds may lead to novel phenomena. Furthermore Komatsu et al. have recently succeeded in almost 100% encapsulation of H_2 into the cage by means of organic synthesis.[80,81] These accomplishments will open a new field in the study of endohedral fullerenes that give rise to novel dynamic functionality due to thermal fluctuation, since such small molecules can move inside the cage and affect the electronic structure of the cage and are affected by the cage.

Be endohedral fullerene is generated by recoil nuclear reactions rather than by conventional ion implantation,[82] whose generation was also investigated in detail by first principle calculation. Türker performed calculations of energy and an effective charge on Be and hydrogen molecules in endohedral fullerenes using semiempirical calculation.[83] Although beryllium is a metallic element, the author found that the effective charge on Be in C_{60} fullerene is slightly negative and becomes positive when two more H_2 molecules are encapsulated. Moreover Be position in the optimized structure of Be@C_{60} using AM1 is on-center. However, it is expected that the structure and effective charges on atoms remarkably vary with a change of the environment such as interactions with other molecules and temperature.

Here we demonstrate the electronic structural change of confined species due to motions in the cage coupled with the motion of cage itself. A gigantic charge fluctuation is observed when the number of confined species increase, and the fluctuation becomes more remarkable with the applied temperature increase. First we explain the theoretical background to treat the system. Second the potential energy surface (PES) of the Be endohedral fullerene and the electronic structure change along the PES are investigated. Finally we perform quantum mechanical (QM)/molecular mechanics (MM) molecular dynamics simulation of the systems in order to observe the thermal fluctuation of the electronic structure of Be inside the cage.

2.1 Theoretical Background. With the development of computer facilities and computing methods, large molecular

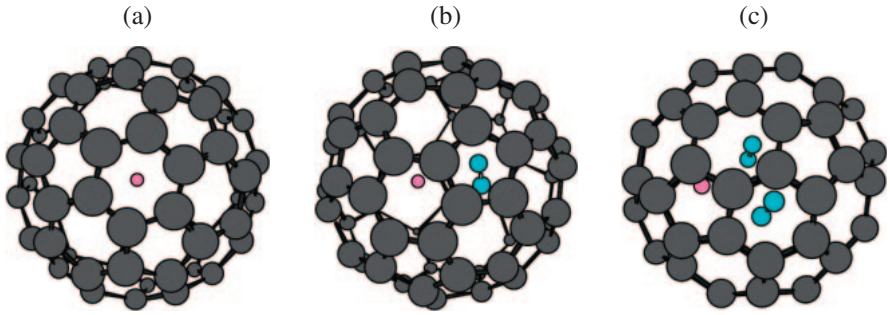

Figure 1. Model systems: optimized structures of (a) Be@C_{60}, (b) (Be + H_2)C_{60}, and (c) (Be + $2H_2$)C_{60} at AM level.

systems such as proteins can be studied by QM methods that are treated mainly using Hartree–Fock (HF), density functional theory (DFT), or semiempirical models. It is however not possible to use first principle QM methods, i.e., HF and DFT, and even semiempirical methods for describing whole condensed systems and for performing long time dynamics because of computational limitations. QM/MM models have been developed to avoid these limitations and to take the merits of both the quantum and classical approaches.[84] The efficiency and accuracy of QM/MM models are closely related to the QM and the MM potentials. In this work, we employ semiempirical methods to the QM region and all-atom force field MM2 parameterization to the MM region,[85] respectively.

In QM/MM calculations a model Hamiltonian is divided into three components:

$$\hat{H} = \hat{H}_{\mathrm{QM}} + \hat{H}_{\mathrm{QM/MM}} + H_{\mathrm{MM}} \tag{1}$$

where H_{QM} is the QM Hamiltonian operator, H_{MM} is the classical MM Hamiltonian, and $H_{\mathrm{QM/MM}}$ is the coupling term between QM and MM regions. In conventional QM/MM treatment, the QM/MM Hamiltonian consists of an electrostatic interaction between the MM and the QM portions plus a van der Waals (vdW) term. Since the MM2 Hamiltonian does not include the electrostatic term, we need to construct the QM/MM interaction. In conventional QM/MM methods, charge equilibration (QEq)[86] is sometimes used to determine the partial charges on the MM atoms or constant charge MM model is applied. In this work, effective charges on the MM atoms are replaced by QM Mulliken charges which are determined by QM calculation. The QM/MM interaction term in the present model is given by

$$\begin{aligned}\hat{H}_{\mathrm{QM/MM}} &= \sum_{i,M}\frac{q_M}{r_{i,M}} + \left(\sum_{Q,M}\frac{Q_Q q_M}{R_{Q,M}} + E^{\mathrm{vdW}}_{\mathrm{QM/MM}}\right) \\ &= \hat{H}^{\mathrm{ele}}_{\mathrm{QM/MM}} + E^{\mathrm{nuc}}_{\mathrm{QM/MM}}\end{aligned} \tag{2}$$

where Q_Q and q_M denote nuclear charge on the QM atom and an effective charge on the MM atom, respectively, and $r_{i,M}$ ($R_{Q,M}$) is the distance between i-th electron (Q-th QM nucleus) and the MM atom. In the above equation, subscripts Q and M denote QM and MM atoms, respectively. The electronic structure of the QM/MM model is determined via the Schrödinger equation

$$(\hat{H}_{\mathrm{QM}} + \hat{H}_{\mathrm{QM/MM}})\Psi = (E^{\mathrm{ele}}_{\mathrm{QM}} + E^{\mathrm{ele}}_{\mathrm{QM/MM}})\Psi = E^{\mathrm{ele}}\Psi \tag{3}$$

The total energy of the QM/MM model is given by

$$E^{\mathrm{T}} = E^{\mathrm{ele}} + E^{\mathrm{nuc}}_{\mathrm{QM/MM}} + E_{\mathrm{MM}} \tag{4}$$

where E^{T} and E_{MM} is total energy and the energy of MM portions, respectively. In the optimized structure calculation and molecular dynamics simulation, the gradients on both atoms are described as

$$\begin{aligned}\frac{\partial E^{\mathrm{T}}}{\partial \mathbf{R}_Q} &= \left[\frac{\partial E^{\mathrm{el}}}{\partial \mathbf{R}_Q} + \frac{\partial E^{\mathrm{nuc}}_{\mathrm{QM/MM}}}{\partial \mathbf{R}_Q}\right] \\ \frac{\partial E^{\mathrm{T}}}{\partial \mathbf{R}_M} &= \left[\frac{\partial E_{\mathrm{MM}}}{\partial \mathbf{R}_M} + \frac{\partial E_{\mathrm{QM/MM}}}{\partial \mathbf{R}_M}\right]\end{aligned} \tag{5}$$

where $E_{\mathrm{QM/MM}} = E^{\mathrm{ele}}_{\mathrm{QM/MM}} + E^{\mathrm{nuc}}_{\mathrm{QM/MM}}$.

2.2 Application 1: Static and Dynamic Changes due to Be Atom Confined in Fullerene Cage. Here we first remark on the numerical detail of the present computations. Model systems treated here are depicted in Figure 1. At first we calculate the potential energy curve of Be endohedral fullerene with spin singlet state ($S = 0$) at the DFT level using Gaussian.[87] We employ the B3LPY hybrid exchange-correlation functional and 6-31G(2d,2p) basis sets for the DFT calculations. We here fix the C_{60} cages at the icosahedral symmetry (I_h) with two characteristic bond lengths, $R_{\mathrm{C-C}} = 1.453$ and $R_{\mathrm{C=C}} = 1.367$ Å, respectively. These bond lengths are optimized by using B3LYP level with 6-31G(2d,2p).

Then, QM/MM MD simulations are carried out only at the AM1 level[88] using a modified version of GAMESS.[89] As an initial geometry the optimized structures of (Be + $n$$H_2$)Be@$C_{60}$ ($n = 1$ and 2) with $S = 0$ at the AM1 level are utilized. The simulation conditions are $\mathrm{d}t = 0.20$ fs and $T = 100$–300 K by employing a massive Nosé–Hoover chain.[90] After 1 ps equilibration has been carried out, the subsequent 9 ps simulations have been performed to calculate ensemble averages. One (Be + $n$$H_2$)@$C_{60}$ is placed in a simple cubic cell ($a = 14.520$ Å) for low temperature cases (below 260 K) and in an fcc cell ($a = 14.154$ Å) for high temperature (above 260 K). These lattice constants are assumed to be the same as those of C_{60}. Here we treat the neighborhood MM molecules as replicated images of the QM molecule instead of imposing the periodic boundary condition.[85] We set a cut-off length at 30 Å. For the MM interactions the MM2 parameter set of the van der Waals interactions is used.[91] Under the present AM1-QM/MM model, the NDDO (neglect of diatomic differential overlap) approximation is adopted for the QM/MM electrostatic interactions, where the effective charges on the MM atoms are replaced by the QM Mulliken charges.

We first set the center of mass (COM) of the C_{60} as the origin and define the distance from Be (H) to COM as $R_{Be–COM}$ ($R_{H–COM}$). In Figure 2 the energy differences are illustrated as a function of $R_{Be–COM}$ for two different directions. One is the direction toward the center of the 5-membered ring from the center of the C_{60} cage, and the other is that toward the center of 6-membered ring. We hereafter refer them as $\boldsymbol{d}_5$ and $\boldsymbol{d}_6$ directions, respectively, and adopt them as the z axis. From Figure 2, we found that there are small differences between energy along $\boldsymbol{d}_5$ and $\boldsymbol{d}_6$ directions for a long distance. The potential energies obtained by both methods gradually increase. These potentials indicate that the position of the Be at optimized structure is the center of the cage as pointed out in the introduction. The effective charges on the Be atom, Q_{Be}, first gradually decline and then sharply increase around $R_x = 1.2$ Å ($x = 5$ and 6) for the DFT B3LYP level. Although the AM1 method overestimates Q_{Be} twice as much as those obtained by the DFT B3LYP method, it shows the same tendency. In what follows, we utilize AM1 approximation in order to investigate dynamic changes in Q_{Be} at least qualitatively rather than quantitatively.

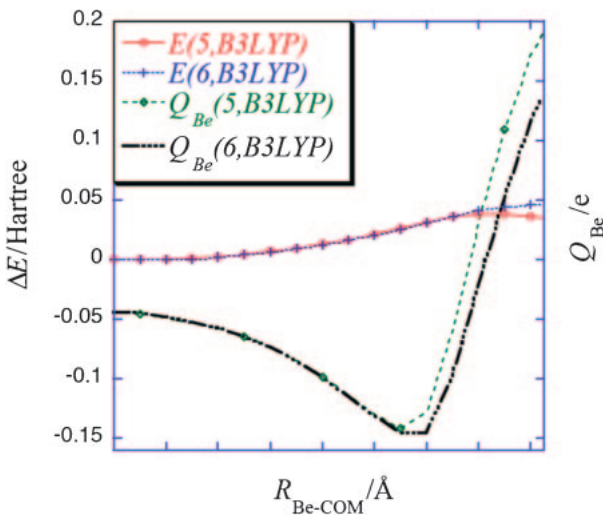

Figure 2. Potential energy surface and effective charge on Be as a function of $R_{Be–COM}$.

In Figure 3, we plot an ordering of the C atoms in the present system and the summation of effective charges on symmetrically equivalent C atoms, ΣQ_{xC}, along the $\boldsymbol{d}_5$ direction besides Q_{Be}. In this case, there exist eight different equivalent sites because of symmetry (C_{5v}). The indices of equivalent C atoms are given in Figure 3b. Especially we hereafter refer the site (5-membered ring), that consists of 1, 2, 3, 4, and 5 C atoms, to a first layer. A summation of the effective charges on the first layer is defined as ΣQ_{1C}.

According to Figure 3b, it is clearly found that ΣQ_{1C} is negative and ΣQ_{xC} positive at $R_{Be–COM} = 0$. With increase of $R_{Be–COM}$, ΣQ_{1C} decreases and others increase gradually at first. Parts of ΣQ_{xC} turn to decrease one after another at around 1.2 Å, because the interactions between Be and other layers become strong as distances from Be to C atoms shorten. Finally the effective charge on Be becomes positive and ΣQ_{1C} turns to increase around 1.5 Å. Note that those along the $\boldsymbol{d}_6$ direction are omitted, because they show the same tendency. Nevertheless the symmetry of this case (C_{3v}) is lower than that of the former so that the number of equivalent sites increases.

The Be atomic 1s levels lie upon all C atomic 1s levels, that is to say the 61st orbital is mainly due to the Be 1s orbital. On the other hand, the Be atomic 2s level lies between the highest occupied molecular orbital (HOMO) and the lowest unoccupied molecular orbital (LUMO). The HOMO–LUMO gap of this compound is estimated to be 2.53 eV. Figure 4a illustrate variations of the orbital energies along the $\boldsymbol{d}_5$ direction. Note that those along the $\boldsymbol{d}_6$ direction are also omitted because of the same tendency. Although the total energy does not change at around 1.2 Å, from the top panel of Figure 4a the 61st orbital energy initially increases and begins to decrease drastically at this point. This behavior is quite similar to that of the effective charge on Be. The orbital energy of the HOMO increases and becomes almost constant at almost the same point. In comparison with large deviation in the HOMO, the second HOMO and LUMOs gradually increase or decrease. Initially LUMOs are threefold degenerate at $R_{Be–COM} = 0$ and split into two bands. One of them decreases and the other increases with increase of $R_{Be–COM}$. Consequently the HOMO–LUMO gap is reduced to -0.743 eV at $R_{Be–COM} = 1.6$ Å.

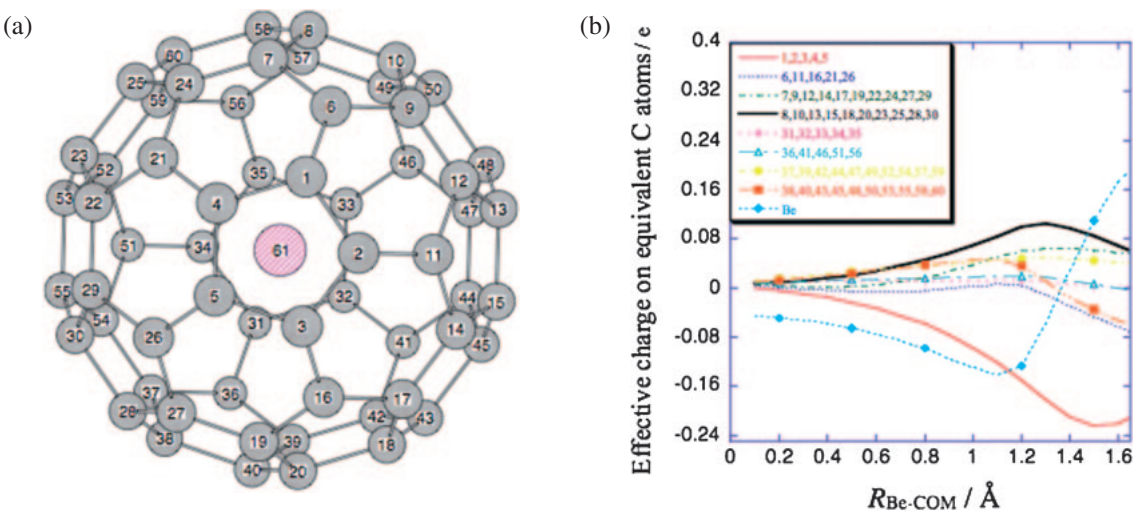

Figure 3. Effective charge in Be@C_{60} as a function of $R_{Be–COM}$.

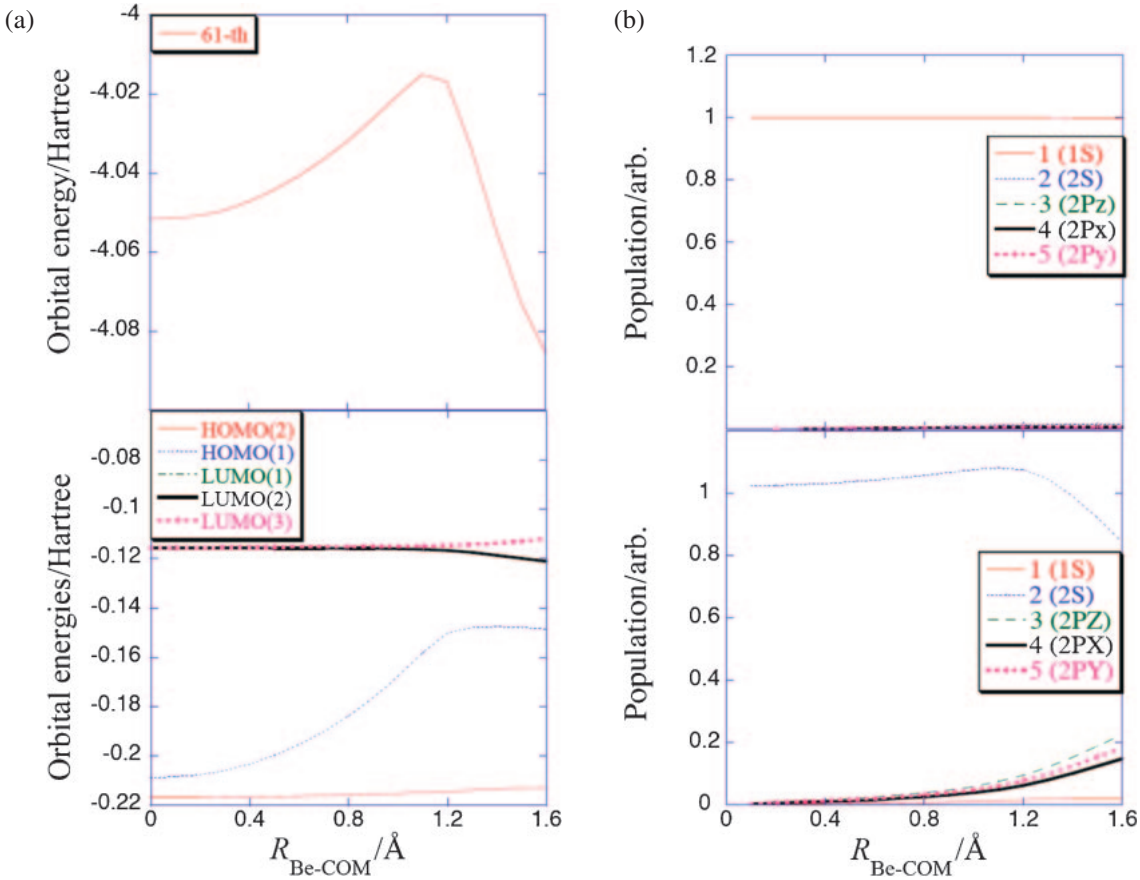

Figure 4. (a) Orbital energy shift and (b) overlap of orbitals as a function of $R_{Be\text{–}COM}$.

To understand the polarization effect on the Be atomic orbital affected by the cage, we plot the absolute value of overlap between Be atomic orbials and Be atomic orbitals in the cage in Figure 4b. The upper panel of Figure 4b shows that the 1s component of the 61st molecular orbital does not change with increase of $R_{Be\text{–}COM}$ due to screening effects of components of Be 2s and 2p orbitals of the HOMO. On the other hand the 2s AO component of the HOMO first gradually increases and change to decrease at around 1.2 Å. On the contrary 2p AO components monotonically increase. In particular the population of $2p_z$ component is larger than those of the $2p_x$ and $2p_y$ components. It is found that curvature of the 2p components vary also at 1.2 Å. These results indicate that Be is largely polarized by the influence of the cage when the Be atom near to the cage. Therefore we expect that properties of Be in the cage largely vary with the influence of other encapsulated molecules and motion of the Be atom interacting with the cage and other molecules. In the following we investigate these two effects of the encapsulated system. One is number effects of encapsulated molecules and the other is dynamic effects on the effective charge on Be.

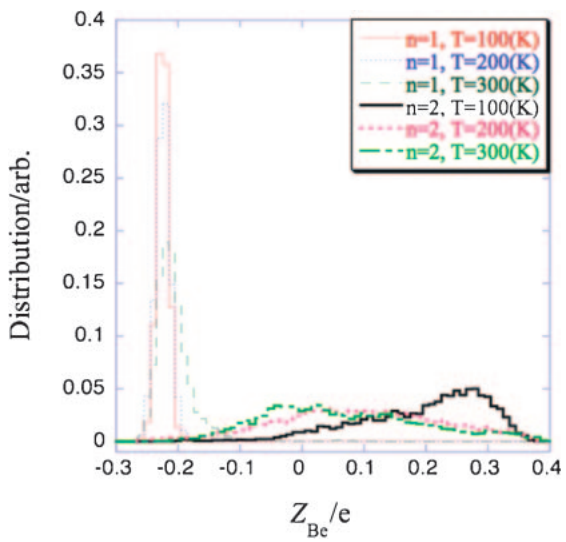

Figure 5. Distribution of charge for different number of H_2, n, and temperature, T.

Next we proceed to the dynamic properties of the system encapsulating both Be and hydrogen molecules. The main findings in our simulation study are visually summarized in Figure 5, which shows the frequency distribution of Q_{Be} as a function of n and T. (i) A dramatic difference between $n = 1$ and $n = 2$ is observed; Q_{Be} for $n = 1$ is negative for all the temperatures studied, while that for $n = 2$ at $T = 100$ is positive. (ii) Q_{Be} for $n = 1$ is almost constant for all the temperatures under study. (iii) Furthermore, Q_{Be} for $n = 2$ has a very wide distribution, and the peak position is significantly shifted to a lower value as the temperature is changed from $T = 100$ to $T = 200$. Such a large shift is not observed between $T = 200$ and $T = 300$ despite the difference in the crystal structure between these temperatures.

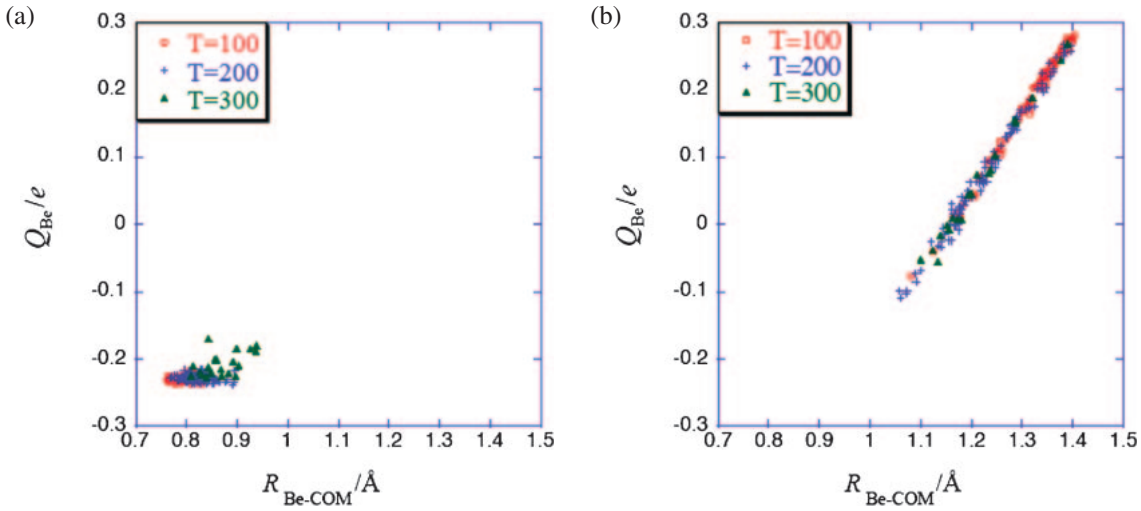

Figure 6. Correlation of Q_{Be} and $R_{Be\text{–}COM}$ for (a) $n = 1$ and (b) $n = 2$.

Figure 6 exhibits the correlation between the short-time averages taken at every 0.1 ps of $R_{Be\text{-}COM}$ and Q_{Be} for $n = 1$ and 2 in Figures 6a and 6b, respectively. Figure 6a clearly shows that the system of $n = 1$ undergoes a very small fluctuation for all the temperatures studied. On the other hand, Figure 6b indicates that Q_{Be} of $n = 2$ widely fluctuates almost linearly with $R_{Be\text{–}COM}$. However, the slope of this linearity virtually does not depend on the temperature. Thus we see that the fluctuation of Q_{Be} is predominantly driven by the change of $R_{Be\text{–}COM}$.

In conclusion, we have shown that the effective charge on Be undergoes a large time-dependent fluctuation, which is driven by the positional change of Be atom. It is well known in molecular science that the HOMO–LUMO gap of a small molecule is usually so large that electronic fluctuation due to the mixing of the excited states is not induced by such a small perturbation. In particular, Be has a quite stable electronic structure, namely, $1s_2$–$2s_2$. Therefore such a large thermal fluctuation at low temperature is very astonishing, which should reflect a truly characteristic nature of the 3D reaction field inside the cage.

3. Theoretical Development of Quantum Effects of Nuclei

As mentioned in the introduction, we have developed two different theories in order to treat nuclear quantum effects. One is wave function based and the other is operator (or expectation value) based. For the former theory, we generalized Thomas' protonic structure concept[92] to polyatomic systems by means of a linear combination of both electronic and nuclear one-particle orbitals. At first we adopted a generator coordinate method to estimate electronic and vibronic excited states,[22] and then reformulated by using non-Born–Oppenheimer density functional theory (NBO-DFT)[23] and Green's function theory.[24] Nakai and Tachikawa also derived the same methodology at almost the same time[34] and developed post self-consistent field methods. They referred to these methods as multicomponent molecular orbital (MCMO) or nuclear orbital plus molecular orbital (NOMO) method.[25–43] Later Hammes-Schiffer and her collaborators applied these methods to chemically interesting systems such as proton transfer in malone aldehyde and some biological molecules.[44–56] Their group implemented the methods to the GAMESS program package.[89]

The later theory is based on the Heisenberg equation of motion, which is equivalent to the time-dependent Schrödinger equation. This theory was established immediately after the Schrödinger equation was formulated. In 2001, Prezhdo and his group developed a Heisenberg equation of motion (EOM)-based approach, where they use moments of coordinate and momentum operators as central variables.[57] Nevertheless the method had drawbacks when applied to a general potential. In order to remove the drawbacks, we have utilized the cumulant rather than the moment as a dynamic variable.[63–68] We refer to the method as QCD. The cumulant expansion techniques were introduced by Mayer for classical problems[93] and Kubo[94] for quantum mechanical problems to evaluate averages of exponential functions. The advantages of the cumulant expansion over the moment expansion are as follows: (i) one can avoid tedious derivation in the decomposition so that there is no need to truncate the given potential; (ii) fewer terms appear than in the moment expansion as shown later. Recently, cumulant expansion has been applied by several groups to quantum chemistry problems in relation to higher-order density matrices[95,96] and to multireference coupled cluster methods.[97] The cumulant-based theory is also given by Mukherjee for thermal averages.[98]

In what follows, we introduce two theories and their applications. For the former, we demonstrate how the electronic densities and bond lengths of small molecules with the NBO treatment deviate from those obtained by conventional BO treatment. For the latter, normal mode analysis for the vibrational motion is extended and the vibrational frequencies obtained by classical MD was compared with those obtained by the new methodology, i.e., QCD.

3.1 Theoretical Background of Non-Born–Oppenheimer Density Functional Theory (NBO-DFT). Recent state of the art electronic structure calculation is based on density functional theory,[99,100] which is successful in many fields of science (see Ref. 101). First, NBO-DFT, especially electron- and nuclear-coupled Kohn–Sham (KS) equations, is briefly reviewed. The formulation of coupled KS equations is an

extension of work by Capitani, Kryachko, and Gidopoulos to multicomponent systems.[102–104]

The full Hamiltonian H for a molecular system consisting of N electrons and M nuclei is given as atomic unit and is used throughout in this text

$$\hat{H} = \sum_i \left(-\frac{\nabla_i^2}{2}\right) + \sum_i \left(-\frac{\nabla_a^2}{2M_a}\right) + \frac{1}{2}\sum_{i\neq j}\frac{1}{|\mathbf{r}_i - \mathbf{r}_j|} + \frac{1}{2}\sum_{a\neq b}\frac{Z_a Z_b}{|\mathbf{R}_a - \mathbf{R}_b|} - \sum_{i,a}\frac{Z_a}{|\mathbf{r}_i - \mathbf{R}_a|} \quad (6)$$

where $\mathbf{r}_i$ and $\mathbf{R}_a$ are the coordinate for i-th electron and for a-th nucleus, respectively. Z_a and M_a denote the atomic number of a-th nucleus and its mass. One defines one particle density for an electron with spin σ

$$\rho_\sigma(\mathbf{r}_1) = \int |\Psi(\{\mathbf{r}_i\sigma_i, \mathbf{R}_\alpha, \Sigma_\alpha\})|^2 \mathrm{d}\tau \quad (7)$$

and an α-type nucleus with $I \equiv \Sigma_\alpha$ spin

$$P_I(\mathbf{R}_\alpha) = \int |\Psi(\mathbf{r}_i\sigma_i, \mathbf{R}_\alpha\Sigma_\alpha)|^2 \mathrm{d}\tau' \quad (8)$$

where $\Psi(\{\mathbf{r}_i\sigma_i, \mathbf{R}_\alpha, \Sigma_\alpha\})$ is an exact ground state of a given system. $\mathrm{d}\tau$ ($\mathrm{d}\tau'$) denotes the product form of all spin-space volume elements except for $\mathrm{d}\mathbf{r}_1\mathrm{d}\sigma_1$ ($\mathrm{d}\mathbf{R}_\alpha\mathrm{d}\Sigma_\alpha$).

We now define a ground state energy density functional for the NBO case as

$$E[\{\rho_\sigma(\mathbf{r})\}, \{P_I(\mathbf{R})\}] = \min\langle\Psi_{\{\rho_\sigma(\mathbf{r})\},\{P_I(\mathbf{R})\}}|\hat{H}|\Psi_{\{\rho_\sigma(\mathbf{r})\},\{P_I(\mathbf{R})\}}\rangle \quad (9)$$

E searches all wave functions in the domain of the full Hamiltonian of eq 6, $\hat{H}$ of appropriate symmetries, and the statistics of particles. Next, we define two functionals as follows:

$$\tilde{E}[\{\rho_\sigma(\mathbf{r})\}, \{P_I(\mathbf{R})\}] = \min_{\Psi\to\{\rho_\sigma(\mathbf{r})\},\{P_I(\mathbf{R})\}}\langle\Psi|(\hat{T}_e + \hat{T}_n + \hat{V}_{ee} + \hat{V}_{nn} + \hat{V}_{en})|\Psi\rangle \quad (10)$$

$$E_0[\{\rho_\sigma(\mathbf{r})\}, \{P_I(\mathbf{R})\}] = \min_{\{\chi\}\to\{P_I\}}\langle\chi|\hat{T}_n|\chi\rangle + \min_{\{\phi\}\to\{P_\sigma\}}\langle\phi|\hat{T}_e|\phi\rangle \quad (11)$$

where the minimization of $\tilde{E}$ searches over all Ψ which is obtained from $(\{\rho_\sigma(\mathbf{r})\}, \{P_I(\mathbf{R})\})$, while the minimization of E_0 searches over a N-particle Slater determinant for electrons, and the product of M-particle Slater determinants for fermionic nuclei and/or permanents for bosonic nuclei, which are obtained from $(\{\rho_\sigma(\mathbf{r})\}, \{P_I(\mathbf{R})\})$ as

$$|\phi\rangle = \det|\{\phi_{i\sigma}(\mathbf{r})\}|$$
$$|\chi\rangle = \prod_\alpha |\chi_\alpha\rangle \quad (12)$$

with

$$|\chi_\alpha\rangle = \begin{cases} \det|\{\chi_{\alpha\Sigma}(\mathbf{R})\}| & \text{fermion} \\ \mathrm{per}|\{\chi_{\alpha\Sigma}(\mathbf{R})\}| & \text{boson} \end{cases} \quad (13)$$

where det and per mean the determinant for the fermion and the permanent for the boson, respectively.

We assume that there is a state, which minimize the above functionals. We define one-particle orbitals, which minimize the above functionals.

$$\tilde{E}[\{\rho_\sigma(\mathbf{r})\}, \{P_I(\mathbf{R})\}] = \langle\Psi_{\{\rho_\sigma(\mathbf{r})\},\{P_I(\mathbf{R})\}}|(\hat{T}_e + \hat{T}_n + \hat{V}_{ee} + \hat{V}_{nn} + \hat{V}_{en})|\Psi_{\{\rho_\sigma(\mathbf{r})\},\{P_I(\mathbf{R})\}}\rangle \quad (14)$$

$$E_0[\{\rho_\sigma(\mathbf{r})\}, \{P_I(\mathbf{R})\}] = \langle\chi_{\{P_I(\mathbf{R})\}}|\hat{T}_n|\chi_{\{P_I(\mathbf{R})\}}\rangle + \langle\phi_{\{\rho_\sigma(\mathbf{r})\}}|\hat{T}_e|\phi_{\{\rho_\sigma(\mathbf{r})\}}\rangle \quad (15)$$

We now define the exchange-correlation energy functional as

$$E_{xc}[\{\rho_\sigma(\mathbf{r})\}, \{P_I(\mathbf{R})\}] = \tilde{E}[\{\rho_\sigma(\mathbf{r})\}, \{P_I(\mathbf{R})\}] - E_0[\{\rho_\sigma(\mathbf{r})\}, \{P_I(\mathbf{R})\}] \quad (16)$$

The KS functional for the molecular system is derived as

$$E[\phi, \chi] = \langle\phi|\langle\chi|(\hat{T}_e + \hat{T}_n)|\chi\rangle|\phi\rangle + E_{xc} + \frac{1}{2}\iint\frac{\rho(\mathbf{r})\rho(\mathbf{r}')}{|\mathbf{r} - \mathbf{r}'|}\mathrm{d}\mathbf{r}\mathrm{d}\mathbf{r}' - \sum_a Z_a\iint\frac{P_a(\mathbf{R})\rho(\mathbf{r})}{|\mathbf{r} - \mathbf{R}|}\mathrm{d}\mathbf{r}\mathrm{d}\mathbf{R} + \frac{1}{2}\sum_{a,b}Z_a Z_b\iint\frac{P_a(\mathbf{R})P_b(\mathbf{R}')}{|\mathbf{R} - \mathbf{R}'|}\mathrm{d}\mathbf{R}\mathrm{d}\mathbf{R}' \quad (17)$$

where $E[\phi, \chi]$ is the functional of orbitals $\phi_{i\sigma}$ and $\chi_{a\Sigma}$, because noninteracting states ϕ and χ are constructed by the Slater determinants or permanents which consists of these orbitals. If the orbitals minimize the functional, we obtain the electron and nuclear coupled KS equations as

$$\hat{F}_\sigma\phi_{i\sigma}(\mathbf{r}) = \left[-\frac{\nabla^2}{2} + V_H(\mathbf{r}) + V_{xc}^\sigma[\mathbf{r}; \rho, P]\right] = \varepsilon_{i\sigma}\phi_{i\sigma}(\mathbf{r}) \quad (18)$$

$$\hat{F}_{a\Sigma}\chi_{ja\Sigma}(\mathbf{R}) = \left[-\frac{\nabla^2}{2M_a} - Z_a V_H(\mathbf{R}) + V_{xc}^{a\Sigma}[\mathbf{R}; \rho, P]\right] = E_{ja\Sigma}\chi_{ja\Sigma}(\mathbf{R}) \quad (19)$$

where $\hat{F}_\sigma$ ($\hat{F}_{a\Sigma}$) and $\varepsilon_{i\sigma}$ ($E_{a\Sigma}$) are the KS operator and corresponding i-th (j-th) eigenvalue for an electron with spin σ (the a-type nucleus with the spin Σ). The classical Coulomb potential Hartree potential is given by

$$V_H(\mathbf{r}) = \int\frac{\sum_\sigma\rho_\sigma(\mathbf{r}')}{|\mathbf{r} - \mathbf{r}'|}\mathrm{d}\mathbf{r} - \int\frac{\sum_{b\Sigma}Z_b P_{b\Sigma}(\mathbf{R})}{|\mathbf{r} - \mathbf{R}|}\mathrm{d}\mathbf{R} \quad (20)$$

While the exchange-correlation potential for the electron and nucleus are defined as

$$V_{xc}^\sigma[\mathbf{r}; \rho, P] = \frac{\delta E_{xc}[\rho, P]}{\delta\rho_\sigma(\mathbf{r})} \quad (21)$$

$$V_{xc}^{a\Sigma}[\mathbf{R}; \rho, P] = \frac{\delta E_{xc}[\rho, P]}{\delta P_{a\Sigma}(\mathbf{R})} \quad (22)$$

where $\rho_\sigma(\mathbf{r})$ and $P_{a\Sigma}(\mathbf{R})$ denote the densities of electron and nucleus, respectively, as follows:

$$\rho_\sigma(\mathbf{r}) = \sum_i f_{i\sigma}|\phi_{i\sigma}(\mathbf{r})|^2 \quad (23)$$

$$P_{a\Sigma}(\mathbf{R}) = \sum_j f_{ja\Sigma}|\chi_{ja\Sigma}(\mathbf{R})|^2 \quad (24)$$

The coupled electron and nuclear exchange-correlation functional is constructed by approximating the two-body density matrix on the same basis of Colle–Salvetti type

functional by Nakai's group.[33] Since the nuclear–nuclear correlation mostly consists of self-interaction error and the nuclear–electronic correlation originates from a cusp between electrons and nuclei, the most important component of the chemical problems is still electron–electron correlation so Tachikawa and Hammes-Schiffer adopted the electron–electron correlation only.[39,54]

If we replace the exchange-correlation potential by the HF exchange (or permutation) operator, we can easily obtain a coupled electron and nuclear HF equation. In the latter numerical application, the exchange-correlation energy functional is appropriately treated as HF exchange and the nuclear–electronic correlation is neglected for simplicity.

3.2 Application 2: Protonic Structure of an Amino Acid. Recently the number of protein crystal structures determined by X-ray experiments, resolution and size of protein being analyzed has been increasing year by year.[105] Nevertheless determination of the positions of hydrogen atoms is still a problem, since the resolution is insufficient. This problem is crucial for protonatable amino acids and hydrogen-bonding networks, since these often play biologically relevant role. In order to observe hydrogen atoms in proteins and surrounding hydrated water molecules, one still seeks to develop ways to obtain pure, large crystals, to get high intensity X-rays, and to refine diffraction patterns obtained by X-ray experiments.

Neutron scattering is a powerful method to since the neutrons are scattered not by electrons as in X-ray experiments but by nuclei so that this technique enables determination of both position of the hydrogen atom in water molecules and orientation. Chatake et al. observed dynamic features of a nuclear density map determined at 1.5–1.6 Å resolution.[106] The data obtained by neutron scattering includes nuclear quantum effects so that the nuclear density is delocalized due to zero point vibrational motion. Thus the obtained nuclear density and corresponding electron density observed in actual experiments will include nuclear quantum effects.

Here we estimate how the nuclear quantum effects affect the bond length and electron densities for a histidine (His) and protonated histidine (Hip), which is the most fundamental protonatable amino acid. Here we apply the NBO-based method to evaluate the electron densities and the interatomic distances of His and Hip (Figure 7) including the nuclear quantum effects. We optimized the structure by BO and NBO HF methods, where the 6-31G for electrons and 4-31G basis set for nuclei are adopted for calculation. In the NBO treatment, the heavy atoms such as C, N, and O atoms are fixed at the optimized structure evaluated by BO treatment. In the calculations the original code is used and a contracted 2s basis for the proton was taken from a previous paper.[24]

Table 1 shows the optimized bond lengths within the BO treatment and the expectation value of the bond length within the NBO treatment. All the bond lengths obtained by NBO treatment are larger than those by BO treatment. The ratio between BO and NBO value is at most about +2.3%. In comparison with His and Hip, the differences in Hip (+2.14–2.29%) are slightly larger than that in His (+2.01–2.14%). Since the protonated histidine is positively charged, the bond lengths of the protons become longer and each bond becomes weaker. In these cases, zero-point vibrational effects become

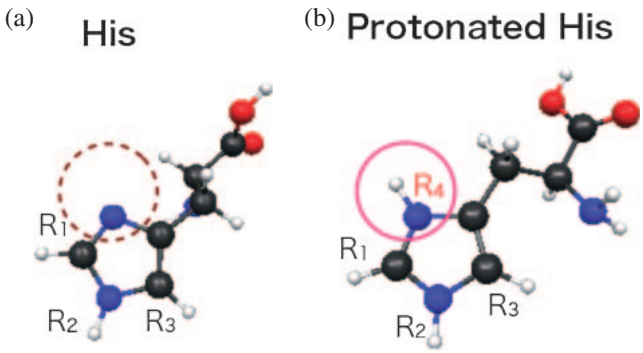

Figure 7. Model systems: (a) histidine (His) and (b) protonated histidine (Hip).

Table 1. C–H and N–H Bond Distances in Histidine (His) and Protonated Histidine (Hip) by means of BO HF/6-31G and NBO HF/6-31G (Electron) and 4-31G (Proton) Treatments (in Å)[a)]

	BO R_{eq}	NBO R_0	BO R_0	Ratio (BO R_{eq}/NBO R_0) /%
His R_1	1.065	1.087	1.090	+2.08
His R_2	0.990	1.011	1.014	+2.14
His R_3	1.065	1.086	1.090	+2.01
Hip R_1	1.065	1.088	1.090	+2.15
Hip R_2	0.995	1.018	1.019	+2.28
Hip R_3	1.062	1.085	1.086	+2.14
Hip R_4	0.995	1.018	1.019	+2.29

a) BO R_0 is evaluated by solving one-dimensional Schrödinger equation on quartic force field for each bond.

remarkable. We can explain the relationship between BO R_e and NBO R_0 by using the PES concept. R_e is the lowest point (basin) of the PES. On the other hand, R_0 is the expectation value averaged over a vibrational ground state. By means of NBO treatment, we can directly obtain R_0 rather than R_e. We also list R_0 values evaluated from approximate one-dimensional Schrödinger equation obtained from a fourth order BO potential energy curve for each bond, where only X–H (X = C or N) distance is treated and other atoms are fixed in this model. The obtained data are also comparable with the NBO results so that the NBO treatment gives R_0 effectively.

Figure 8 shows the electron density differences between the BO and NBO treatments. Note here that the electron density obtained by the NBO treatment is the vibrationally coupled electron density that includes the nuclear quantum effects. It is easily found that there exists explicit difference not only around the position of the protons but also around the heavy elements. Around the protons, the difference is negative so that the electron density decreases due to nuclear quantum effects. The remaining density of the proton is distributed over the molecule. Thus the electron density around some (not all) heavy element increases. The heavy elements with decreased electron density are a result of a redistribution of electron density.

3.3 Theoretical Background of Quantum Cumulant Dynamics. Molecular vibration is a significant feature of molecules, since it gives fundamental information for chemists

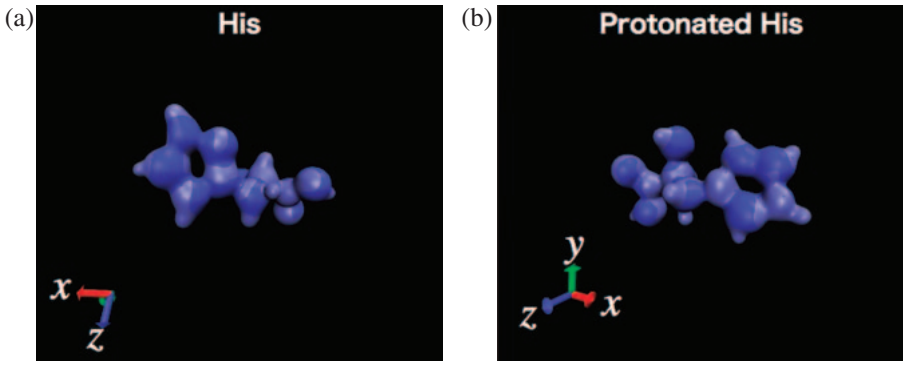

Figure 8. Electron density difference between BO and NBO result ($\rho_{BO}-\rho_{NBO}$), where light-blue-colored.

such as molecular structure and bond strength. It can also be a way to bridge between experimental and theoretical chemistry.[107,108] Recent experimental progress in infrared spectroscopy and Raman spectroscopy, among others, enables one to investigate dynamic aspects of vibrational motion in complex systems such as biomolecules, condensed matter, and bulk systems. To achieve a computationally efficient and accurate method for vibrational analysis of large molecular systems of interest, our viewpoint is focused on utilizing MD simulations. In the MD simulations under the BO approximation, treatment of nuclear motion and accuracy of the PES are the two major issues. For the former issue, a full quantum treatment by solving time-dependent Schrödinger equation is desirable, but the degrees of freedom are limited due to high computational costs.

Instead of the full quantum treatment, classical dynamics is a possible alternative. Direct ab initio MD is now appreciated as a powerful method for studying various chemical interests. It has also been applied to the analysis of molecular vibrations by other groups.[109,110] However, a quantum treatment for the nuclei becomes indispensable for correct description of zero point energy (ZPE) of vibrational modes, of highly excited oscillations such as overtones and combination bands and in cases where the quantum tunneling effect is not negligible.[111,112]

Here we propose a novel method to treat molecular vibration beyond classical treatment and beyond the ordinary normal mode analysis. We first derive a coupled EOM of expectation values from the Heisenberg EOM. Then we define an effective potential energy surface that includes quantum effects. The normal mode analysis (NMA) is extended by introducing a new set of coordinate and momentum, which originate from the quantum effects.

The Hamiltonian of one-dimensional systems is given by

$$\hat{H}(\hat{P},\hat{Q}) = \frac{\hat{P}^2}{2M} + V(\hat{Q}) \tag{25}$$

where the first and second terms are kinetic and potential energy operators, respectively. By introducing the shift operator, an arbitrary operator of the position and momentum operators,

$$A_s(\hat{P},\hat{Q}) = \sum_{m,n} a_{m,n}(\hat{P}^m\hat{Q}^n)_s \tag{26}$$

is rewritten as[12]

$$\langle A_s(\hat{P},\hat{Q})\rangle = \left\langle\left[\exp\left(\delta\hat{Q}\frac{\partial}{\partial q}\right)\exp\left(\delta\hat{P}\frac{\partial}{\partial p}\right)\right]_s\right\rangle A(p,q) \tag{27}$$

where $\delta\hat{A} = \hat{A} - \langle\hat{A}\rangle$ is a definition of a fluctuation operator of a given operator $\hat{A}$ and $\langle\hat{A}\rangle$ is an expectation value of $\hat{A}$. The problem is to evaluate the following expectation value of the symmetric-ordered product of the position and momentum shift operators as

$$D\left(\frac{\partial}{\partial p},\frac{\partial}{\partial q}\right) \equiv \left\langle\left[\exp\left(\delta\hat{Q}\frac{\partial}{\partial q}\right)\exp\left(\delta\hat{P}\frac{\partial}{\partial p}\right)\right]_s\right\rangle \tag{28}$$

The exponential function is also universal and independent of the Hamiltonian. By applying expansion techniques for two variables

$$\ln D\left(\frac{\partial}{\partial p},\frac{\partial}{\partial q}\right) \equiv \sum_{m+n=2}\frac{\lambda_{n,m}}{m!n!}\frac{\partial^{m+n}}{\partial p^m\partial q^n} \tag{29}$$

we have

$$\langle A_s(\hat{P},\hat{Q})\rangle = \exp\left[\sum_{m+n=2}\frac{\lambda_{n,m}}{m!n!}\frac{\partial^{m+n}}{\partial p^m\partial q^n}\right]A(p,q) \tag{30}$$

where we have defined the two-variable cumulant, $\lambda_{n,m}$. For example, lower-order cumulants are expressed by means of expectation values of functions of fluctuation operators as, $\lambda_{1,0}=0$, $\lambda_{2,0}=\langle\delta\hat{Q}^2\rangle$, $\lambda_{3,0}=\langle\delta\hat{Q}^3\rangle$, and $\lambda_{4,0}=\langle\delta\hat{Q}^4\rangle - \langle\delta\hat{Q}^2\rangle^2$. By neglecting higher than second-order terms, the second-order expectation values are given by

$$\langle A_s(\hat{P},\hat{Q})\rangle_2 = \exp\left[\frac{\lambda_{2,0}}{2}\frac{\partial^2}{\partial q^2} + \lambda_{1,1}\frac{\partial^2}{\partial q\partial p} + \frac{\lambda_{0,2}}{2}\frac{\partial^2}{\partial p^2}\right]A(p,q) \tag{31}$$

The second-order energy is approximated as

$$\langle H(\hat{P},\hat{Q})\rangle_2 = \frac{p^2+\lambda_{0,2}}{2M} + \tilde{V}_2(q,\lambda_{2,0}) \equiv E_2(p,q,\lambda_{2,0},\lambda_{0,2}) \tag{32}$$

The energy is a function of the four variables, i.e., the classical momentum and position and the second-order position and momentum cumulant variables. Hereafter we refer to the second-order approximation with respect to the cumulant variables as QCD2.

The quantum mechanical equations of motion for operators are derived from the Heisenberg EOM, which is equivalent to the time-dependent Schrödinger equation. Heisenberg EOM is expressed as

$$i\hbar \frac{\mathrm{d}}{\mathrm{d}t}\langle \hat{A}(t)\rangle = \langle [\hat{A}(t), \hat{H}]_- \rangle \tag{33}$$

Thus the EOMs of the coordinate, momentum, and cumulant variables in the QCD2 framework are

$$\dot{q}(t) = \frac{1}{i\hbar}\langle [\hat{Q}(t), \hat{H}]_- \rangle = \frac{p(t)}{M} \tag{34}$$

$$\dot{p}(t) = \frac{1}{i\hbar}\langle [\hat{P}(t), \hat{H}]_- \rangle = -\tilde{V}_2^{(1,0)}(q(t), \lambda_{2,0}(t)) \tag{35}$$

$$\dot{\lambda}_{2,0}(t) = \frac{1}{i\hbar}\langle [\delta\hat{Q}^2(t), \hat{H}]_- \rangle = \frac{2\lambda_{1,1}(t)}{M} \tag{36}$$

$$\begin{aligned}\dot{\lambda}_{1,1}(t) &= \frac{1}{i\hbar}\langle [[\delta\hat{Q}(t)\delta\hat{P}(t)]_s, \hat{H}]_- \rangle \\ &= \frac{\lambda_{0,2}(t)}{M} - \lambda_{2,0}(t)V_2^{(2,0)}(q(t), \lambda_{2,0}(t))\end{aligned} \tag{37}$$

and

$$\begin{aligned}\dot{\lambda}_{0,2}(t) &= \frac{1}{i\hbar}\langle [\delta\hat{P}^2(t), \hat{H}]_- \rangle \\ &= -2\lambda_{1,1}(t)V_2^{(2,0)}(q(t), \lambda_{2,0}(t))\end{aligned} \tag{38}$$

Note that the second-order position-momentum cumulant, $\lambda_{1,1}(t)$, has been introduced, though the energy is independent of $\lambda_{1,1}(t)$. It is easily shown that the time derivative of the energy is zero, $\dot{E}_2(t) = 0$, so that the energy conserves during the dynamics. Here we have the other conservation law among the cumulant variables.

The time derivative of $\gamma(t) = \lambda_{2,0}(t)\lambda_{0,2}(t) - \lambda_{1,1}^2(t)$ is zero $\dot{\gamma}(t) = 0$, i.e., $\gamma(t)$ is a constant. This indicates that the actual variables in the above five EOMs are reduced to be four. Nevertheless, in this study we use all the EOMs for simplicity.

Although it is quite easy to generalize the methodology to treat multi-dimensional systems, we here do not describe the extension explicitly to avoid verbose explanations (see Ref. 65).

3.4 Application 3: Vibrational Analysis Based on QCD Formalism. We first apply the extended NMA to the one-dimensional Morse Oscillator based on QCD treatment. Since the dimensions of the cumulant variables are different from those of classical ones, we should introduce alternative variables in order to consider the combined normal coordinates that consist of q and $\lambda_{2,0}$. The coordinate and conjugate momentum given from are given by

$$q_\lambda = \sqrt{\lambda_{2,0}} \tag{39}$$

$$p_\lambda = \lambda_{1,1}/\sqrt{\lambda_{2,0}} \tag{40}$$

where the dimensions of q_λ and p_λ are the same as those of q and p. By assuming $\gamma(t) \equiv \hbar^2/4$, the effective energy for the one-dimensional system is rewritten as

$$\begin{aligned}\tilde{E}_{\mathrm{eff}}(q,p,q_\lambda,p_\lambda) = \frac{p^2}{2M} + \frac{p_\lambda^2}{2M} + \frac{1}{8Mq_\lambda^2} \\ + \exp\left(\frac{q_\lambda^2}{2}\frac{\partial^2}{\partial q^2}\right)V_M(q)\end{aligned} \tag{41}$$

By means of the Taylor series expansion, the effective energy is approximately given by second-order with respect to q and q_λ as

$$\begin{aligned}\tilde{E}_{\mathrm{eff}}(q,p,q_\lambda,p_\lambda) = \frac{1}{2M}\begin{pmatrix} p & p_\lambda \end{pmatrix}\begin{pmatrix} p \\ p_\lambda \end{pmatrix} \\ + \frac{1}{2}\begin{pmatrix} \bar{q} & \bar{q}_\lambda \end{pmatrix}\begin{pmatrix} \tilde{V}_{qq} & \tilde{V}_{q\lambda} \\ \tilde{V}_{\lambda q} & \tilde{V}_{\lambda\lambda} \end{pmatrix}\begin{pmatrix} \bar{q} \\ \bar{q}_\lambda \end{pmatrix}\end{aligned} \tag{42}$$

where we have used the following abbreviations as

$$\bar{q} = q - q_{\mathrm{opt}} \tag{43}$$

$$\bar{q} = q - q_{\mathrm{opt}} \tag{44}$$

and

$$\tilde{V}_{qq} = \frac{\partial^2 \tilde{V}_{\mathrm{eff}}(q, q_\lambda)}{\partial q^2} \tag{45}$$

$$\tilde{V}_{q\lambda} = \frac{\partial^2 \tilde{V}_{\mathrm{eff}}(q, q_\lambda)}{\partial q \partial q_\lambda} \tag{46}$$

$$\tilde{V}_{\lambda\lambda} = \frac{\partial^2 \tilde{V}_{\mathrm{eff}}(q, q_\lambda)}{\partial q_\lambda^2} \tag{47}$$

where $\tilde{V}_{\mathrm{eff}}(q, q_\lambda)$ is effective quantal potential energy surface (EQPES) of the Morse potential. The optimized coordinates, q_{opt} and $q_{\lambda,\mathrm{opt}}$, are obtained from the variational solutions on this effective potential. By diagonalizing the matrix in eq 42, one yields vibrational frequencies based on the extended NMA, where the lower energy solution corresponds to the corrected vibrational frequency over that obtained from the ordinary NMA. Figure 9 depicts frequencies obtained from the ordinary NMA on PES and from the extended NMA on EQPES as a function of the mass. We also plotted the energy gap between the ground and the first excited state estimated from the exact solution. The behavior of the exact solution is that (i) there exists a peak around $M/\mathrm{au} \approx 1$ and (ii) the energy gap becomes negative for $M/\mathrm{au} < 0.5$ which is a lower bound for the existence of the first excited state. The extended NMA gives more accurate results than the ordinary NMA does. Although the result by the extended NMA is unfortunately inaccurate for $M/\mathrm{au} < 1.5$ compared to the exact results, its behavior is similar. The frequency becomes complex for $M/\mathrm{au} < 0.2$. This behavior corresponds to the nonexistence of the first excited

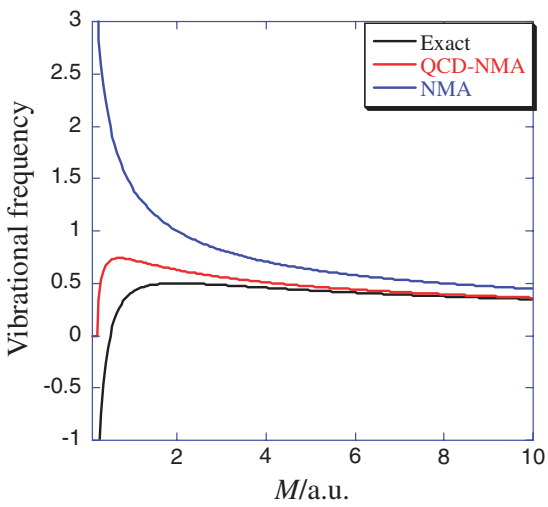

Figure 9. First excitation energy obtained by NMA, QCD-NMA, and exact solution, where negative energy means no solution.

state. On the other hand, the ordinary NMA does not have any peak and the first excited state always exists. Therefore the extended NMA gives reasonable correction to the results obtained from the ordinary NMA as expected.

3.5 Application 4: Estimating Vibrational Spectra from Dynamics. In the previous subsection we consider the extension of the normal mode analysis for the effective potential appearing in the QCD theory. Here we evaluate the vibrational modes from the results obtained from MD simulations. Since the force field based model potentials, which are often used in molecular dynamics simulations, are empirical, they sometimes leads to poor results for molecular vibrations. For quantitative results in any MD study, the accuracy of the PES is an important requirement as well as the treatment of the nuclear motion. Here we use an efficient representation of the PES derived from ab initio electronic structure methods, which is suitable for both molecular vibration and the QCD scheme in principle. In order to include anharmonic effects, multi-dimensional quartic force field (QFF) approximation is applied as

$$V_{\mathrm{QFF}}(\{\hat{Q}_i\}) = V_0 + \sum_i \frac{h_i}{2}\hat{Q}_i^2 + \sum_{ijk}\frac{t_{ijk}}{6}\hat{Q}_i\hat{Q}_j\hat{Q}_k + \sum_{ijkl}\frac{u_{ijkl}}{24}\hat{Q}_i\hat{Q}_j\hat{Q}_k\hat{Q}_l \quad (48)$$

where V_0, h_i, t_{ijk}, and u_{ijkl} denote the potential energy and its second-, third-, and fourth-order derivatives with respect to a set of normal coordinates $\{\hat{Q}_i\}$, at the equilibrium geometry, respectively. To further reduce the computational cost for multi-dimensional cases, an n-mode coupling representation of QFF (nMR-QFF) was applied,[113] which includes mode couplings up to n modes.

The QCD2 and classical simulations were performed numerically with a fourth-order Runge–Kutta integrator. For formaldehyde (CH_2O) and formic acid (HCOOH), 3MR-QFF PES was generated at the level of MP2/aug-cc-pVTZ[114,115] using GAMESS[89] and Gaussian03.[87] In this work, the results obtained by our method are compared with those by vibrational self-consistent field (VSCF) with full second-order perturbation correction (VPT2), which is based on quantum mechanics and accurate enough to treat molecular vibrations.

We here present results of the spectral analysis of trajectories obtained from the simulation that can be compared with other theoretical calculations and experimental results. The Fourier transform of any dynamics variables obtained from the trajectories of MD simulations is related to spectral densities. In particular, Fourier transform of velocity autocorrelation function gives the density of vibrational states. In addition, the power spectrum of the time series or autocorrelation function of each normal coordinate shows the contribution to frequency peaks of the spectrum obtained from velocity autocorrelation. Here we adopted the latter procedure. The time interval used was 0.1 fs and total time is 1 ps for all MD and QCD simulations. The resolution in the frequency domain is less than 1 cm^{-1}, which is sufficient accuracy for analysis of the molecular vibrations of interest. If a longer time trajectory is obtained, the resolution of the Fourier spectrum becomes fine.

Since each normal mode is taken as the degree of freedom explicitly in the present dynamics simulation, the interpretation and analysis of the results can directly be related with each normal mode. The results are shown in Table 2. The table indicates that the harmonic and QFF approximation of the PES results in a large deviation between each other. Therefore, anharmonicity of the potential must be considered to perform reliable simulations. The table shows that for the analysis of fundamental frequencies, the QCD2 has higher accuracy than the classical results, which can be compared with the VPT2 results in all cases. In spite of the high accuracy, the computational cost of the QCD2 remains low even when applied to larger systems. For HCOOH, the QFF is so anharmonic that the classical simulation does not give clear vibrational frequencies due to the chaotic behavior of the power spectrum. The QCD may suppress the chaotic motion as seen in the full quantum mechanics.

Table 2. Vibrational Frequency of H_2CO and HCOOH Molecules[a)]

	Mode	NMA	MD	QCD	VPT2	Exp.
H_2CO	ν_1	3040	2901	2843	2866	2843
	ν_2	2997	2868	2838	2849	2782
	ν_3	1766	1764	1723	1734	1746
	ν_4	1548	1504	1509	1515	1500
	ν_5	1268	1247	1250	1251	1250
	ν_6	1202	1166	N/A	1189	1167
HCOOH	ν_1	3739	N/A	3527	3554	3570
	ν_2	3126	N/A	2980	2989	2943
	ν_3	1794	N/A	1761	1761	1770
	ν_4	1409	N/A	1377	1385	1387
	ν_5	1302	N/A	1270	1231	1229
	ν_6	1130	N/A	1120	1097	1105
	ν_7	626	N/A	631	620	625
	ν_8	1058	N/A	N/A	1036	1033
	ν_9	676	N/A	N/A	642	638

a) N/A means that there are no clear peaks in the power spectrum around corresponding experimental values (in cm^{-1}).

In conclusion of this section, we have developed two different methodologies to treat nuclear quantum effects. The NBO molecular theory was applied to obtain vibrationally coupled electron density of a protonatable amino acid. The obtained results were compared with those obtained from conventional BO results. It was found that the electron density not only around the hydrogen atoms but also around heavy elements differ in comparison with the BO results. We also estimated the bond lengths by means of BO and NBO treatments. The former corresponds to the equilibrium distance, which is the bottom of given PES, while the latter to the expectation value of the vibronic ground state. QCD theory was applied to extend the ordinary NMA, where we introduced the quantum degrees of freedom along with the classical. The new methodology overcomes the breakdown of the ordinary NMA, where any vibrational state does not exist actually, though the NMA predicts its existence. The QCD simulations were performed to evaluate vibrational frequencies from its auto-correlation function. The results were compared with those by classical MD and confirmed the efficiency and superiority of the present method.

4. Grid-Based Density Functional Theory for Electron and Nuclear Dynamics

In order to perform complicated quantum dynamics, the choice of the basis is very crucial. Previously we used a single configuration interaction basis, which consists of a molecular orbital obtained by performing self-consistent field calculations of a linear combination of atomic orbitals. This basis is too compact not to describe precise dynamics. Recently there has been an increasing interest in using uniform grids, wavelet, i.e., real-space grid basis for solving time-independent and dependent Schrödinger equations.[116–132] Real-space grids give an unbiased description of the wave function, and the quality of the description can be controlled by number of grid points. The finite difference scheme is widely used, because the formulation is quite simple and its program is easily parallelized. Here we first introduce basics of the real-space grid-based time-dependent density functional theory (RSTDDFT) and then apply it to time-independent and time-dependent problems.

4.1 Theoretical Background. We mention here details of a calculation scheme using the real-space grid basis. We adopt the higher-order expansions for the kinetic operator by using a uniform grid. We approximate $\nabla^2\phi(\mathbf{r}_I) = \nabla^2\phi(x_i, y_j, z_k)$ as

$$\begin{aligned}\nabla^2\phi(x_i, y_j, z_k) = &\sum_{n_x=-N_h}^{N_h} C_{n_x}\phi(x_i + n_x h, y_j, z_k) \\ &+ \sum_{n_y=-N_h}^{N_h} C_{n_y}\phi(x_i, y_j + n_y h, z_k) \\ &+ \sum_{n_z=-N_h}^{N_h} C_{n_z}\phi(x_i, y_j, z_k + n_z h) \end{aligned} \tag{49}$$

where h is a grid spacing, C_i constants in the differential method, and N_h a positive integer describing the accuracy of this approximation. The accuracy is ordered as $O(h^{2N_k+2})$. With these kinetic operators in eq 49 and the local spin density (LSD) approximation,[133] we can construct a Kohn–Sham equation over the grid. We then yield the time-independent Kohn–Sham equation as

$$\begin{aligned}\hat{F}_{\mathrm{KS}}\phi_i(\mathbf{r}_I) &= \left[-\frac{\nabla^2}{2} + \hat{V}_{\mathrm{ext}}(\mathbf{r}) + \hat{V}_H(\mathbf{r}) + \hat{V}_{\mathrm{xc}}(\mathbf{r})\right]\phi_i(\mathbf{r}_I) \\ &= \varepsilon_i\phi_i(\mathbf{r}_I) \end{aligned} \tag{50}$$

where the first term is one-particle kinetic operator, second is the external potential, third is the Coulomb potential, fourth is the exchange correlation potential, and ε_i in the right hand side of the equation is the orbital energy of the i-th orbital, respectively. The external and Hartree and exchange-correlation potentials acting on a given orbital at $\mathbf{r}_I = (x_i, y_j, z_k)$ are defined as

$$\hat{V}_{\mathrm{ext}}(\mathbf{r})\phi(\mathbf{r}_I) = V_{\mathrm{loc}}(\mathbf{r}_I)\phi(\mathbf{r}_I) + \sum_J V_{\mathrm{nloc}}(\mathbf{r}_I, \mathbf{r}_J)u(\mathbf{r}_J) \tag{51}$$

and

$$[\hat{V}_H(\mathbf{r}) + \hat{V}_{\mathrm{xc}}(\mathbf{r})]\phi(\mathbf{r}_I) = [V_H(\mathbf{r}_I) + V_{\mathrm{xc}}(\mathbf{r}_I)]\phi(\mathbf{r}_I) \tag{52}$$

The external (pseudo) potential consists of local and non-local parts. $V_H(\mathbf{r}_I)$ is a Coulomb potential and $V_{\mathrm{xc}}(\mathbf{r}_I)$ is an exchange-correlation potential for the electron evaluated at each point, $\mathbf{r}_I$. We utilize Troullier–Martins pseudo potential[134] with Kleinman–Bylander separable approximation[135] in the actual calculations. The Coulomb potential is obtained from solving the Poisson equation as

$$\nabla^2 V_H(\mathbf{r}_I) = -4\pi\rho(\mathbf{r}_I) \tag{53}$$

where ρ means total density of the molecular system defined as

$$\rho(\mathbf{r}_I) = \sum_{i\in occ} |\phi_i(\mathbf{r}_I)|^2 \tag{54}$$

For isolated systems, we can yield V_H by solving the Poisson equation by means of the multi-grid method. The exchange-correlation potential is directly evaluated at each point.

For the time-dependent case, we replace the orbital energy by the differential operator with respect to time as an analogy of the time-dependent Schrödinger equation. The time-dependent Kohn–Sham equation is given by

$$-i\frac{\partial}{\partial t}\phi_i(\mathbf{r}, t) = \hat{F}_{\mathrm{KS}}(t)\phi_i(\mathbf{r}, t) \tag{55}$$

Since the density depends on the time, KS Fock operator also depends on the time explicitly. In numerical calculation, the Runge–Kutta method is applied to solve the differential equation. For the laser-driven problems, we also add the external field term to the KS Fock operator. The external field is expressed as

$$E_{\pm}(t) = E_0 s(t)[\cos(\omega t + \varphi)\mathbf{e}_x \pm \sin(\omega t + \varphi)\mathbf{e}_y] \tag{56}$$

where E_0 is intensity of the field and $s(t)$ is a shape function. The circularly polarized laser is a special case where the phase factor is $\varphi = \pi/2$.

The NBO method is also implemented in real-space density functional theory (RSDFT). In the actual numerical calculations, we can obtain the ground state by using the reduction technique which is available from the Taylor expansion of an imaginary time evolution operator,

$$e^{-\beta\hat{F}_\sigma}\phi_{i\sigma}(\mathbf{r}) \approx (1 - \beta\hat{F}_\sigma)\phi_{i\sigma}(\mathbf{r}) \tag{57}$$

$$e^{-\beta\hat{F}_{a\Sigma}}\chi_{ja\Sigma}(\mathbf{R}) \approx (1 - \beta\hat{F}_{a\Sigma})\chi_{ja\Sigma}(\mathbf{R}) \tag{58}$$

where β is fixed at a positive constant value. The normalization condition is applied and the KS Fock matrixes are updated every a few steps. In the following, we demonstrate two applications of RSDFT for (i) NBO problem for hydrogen molecules and (ii) electron dynamics in a molecule under a non-resonant circularly polarized laser plus.

4.2 Application 5: NBO Treatment by RSDFT. We assume that the range of molecular spacing is a cubic box with $L_{\max} = 44.61$ au, and we divide $L_{\max}$ into 128 grids, $N_s = 128$. The grid interval h is, therefore, about 0.3512 au. The corresponding cutoff energy is about 40 au. For an initial single-particle wave function for the H_2 molecule, we set Gaussian functions with an exponent of 21.95 located at $\mathbf{R}_1 = (X_1, Y_1, Z_1) = (62, 64, 64)$ for the up-spin proton and $\mathbf{R}_2 = (X_2, Y_2, Z_2) = (66, 64, 64)$ for the down-spin proton. These exponents for nuclei are determined by the Gaussian based method described before. Parameters for the HD and D_2 are taken by the same way. On the other hand, initial electronic wave functions are set at $\mathbf{r}_1 = (x_1, y_1, z_1) = (62, 64, 64)$ and $\mathbf{r}_2 = (x_2, y_2, z_2) = (66, 64, 64)$ and the exponent 0.271 is used

Table 3. Interparticle Distances of Hydrogen Molecule and Isotopomers (in au)

	H_2	HD	D_2
e–e	2.1156	2.0864	2.0853
e–n	1.7959	1.7716	1.7701
n–n	1.4067	1.4054	1.4052
n–n[a)]	1.4487	1.4422	1.4346

a) Accurate data obtained by means of 524 Gaussian geminal method.[136]

for all isotopomers. Note that the initial wave function for the electrons is put at the same grid point of nuclei and that exponents of the wave function are different from those of nuclei. The intermolecular distance for initial location is almost 1.4 au. We set $N_s = 4$ for the Laplacian operator. The pseudo potential is replaced by a bare Coulomb potential in the calculations of hydrogen molecules.

The average interparticle distance between electron and electron (e–e), electron and nucleus (e–n), and nucleus and nucleus (n–n) is indicated in Table 3. n–n distance obtained by means of a highly accurate method is also listed. All the tendencies of the interparticle distances are $H_2 > HD > D_2$. We should note that the n–n distance does not mean the equilibrium distance R_e which is available from the BOA, but corresponds to the average distance R_0 over a nuclear and electronic ground state as denoted before. Although present n–n distances are underestimated in comparison with those by the highly accurate method, the tendency is the same.

4.3 Application 6: Electronic Current Induced by Circularly Polarized Laser Field. Recent advances in laser technology have opened a new field of attosecond (as) science. In this time scale, we can observe nuclear motions precisely and moreover electronic motions. It is well-known that one electron in a hydrogen atom moves around the nuclei. This motion is characterized as a Kepler orbit, which is the motion of an orbiting body as an ellipse, parabola, or hyperbola in celestial mechanics. The period of the Kepler orbit within a classical approximation is about 150 as so that the electron itself is considered to move the as order. Laser control of Rydberg wave packets demonstrated in Refs. 137–140 stimulates us to control an electron in a molecule by means of a laser. We performed quantum electron dynamics of Mg–porphyrin under a circularly polarized laser pulse and showed that the ring-current induced by the laser can be controlled by choosing the shape. Since the Mg–porphyrin has ring structure, it is natural that the induced current is along the structure. Nevertheless current is also induced in the other structure. This work is motivated by a laser control of enantiomers by means of a circularly polarized laser plus.[141,142] Recently the same group also performed the electron control by a linearly polarized laser.[143,144]

The purpose of this part is to show how the electron fluctuates after applying a few cycle off-resonant circularly polarized UV laser pulses, within a few femtoseconds (fs). Our approach will be demonstrated by quantum electron dynamics for the model system, SiH_4 as a test case. For this purpose, we assume that the system has been pre-oriented in the laboratory-fixed x/y-plane, as indicated in Figure 1 and apply the laser along with z-direction. Since the electrons are confined in the molecule and there is no electron source, total induced current is always zero. Instead we observe an atom-centered current vector defined as

$$\mathbf{I}_A(t) = 2i \sum_{i\in occ} \int \omega_A(\mathbf{r})[\phi_i^*(\mathbf{r},t)\nabla\phi_i(\mathbf{r},t) - \nabla\phi_i^*(\mathbf{r},t)\phi_i(\mathbf{r},t)]\mathrm{d}\mathbf{r} \tag{59}$$

where ω_A is an atom-weight function localized at A th atom, which is referred as Becke's fuzzy cell scheme. We also observed an atom-centered dipole moment vector defined as

$$\mathbf{P}_A(t) = \sum_{i\in occ} \int \omega_A(\mathbf{r})\phi_i^*(\mathbf{r},t)\mathbf{r}\phi_i(\mathbf{r},t)\mathrm{d}\mathbf{r} - Z_A\mathbf{R}_A \tag{60}$$

These quantities are three-dimensional vectors centered at each atom. The current indicates that a direction of electronic motion in a molecule and the moment indicates the deformation of electron distribution around each atom. Therefore both vectors are good indicators to detect the electronic motion in the molecules.

We assume that the range of molecular spacing is a sphere with the radius $R_{max} = 12$ au, where the grid interval h is 0.4 au. The corresponding cutoff energy is about 35 au. We set $N_s = 6$ for the Laplacian operator. The local density approximation is adopted and the Zunger–Perdew exchange correlation functional is utilized. We also use a Troullier–Martins pseudo potential with the Kleinman–Bylander separable approximation. For initial single-particle orbitals for the SiH_4 molecule, we solve the time-independent KS equation before dynamics. The time difference is $\mathrm{d}t = 2$ (as), which is 1000 times smaller than the previous time difference utilized for the molecular dynamics (see Section **2**). After obtaining the initial orbitals, the following circularly polarized electric field is applied.

$$E(t) = E_0 \exp(-(t-t_0)^2/\sigma^2)(\mathbf{e}_y \cos\omega t + \mathbf{e}_z \sin\omega t) \tag{61}$$

weher we set $\omega = 8.0$, $\sigma = 2.0$, $t_0 = 0$, and $E_0 = 0.1$ for the simulation. Total time step is 20 fs. During the dynamics, all the nuclei are fixed.

Figure 10 shows a model system and the total induced dipole moment due to irradiation by the laser plus, where the laser is largely dumped after 2.5 fs. At the initial step, dipole moment is exactly 0 due to the symmetry of the SiH_4 molecule. Since the x component of the field is always 0, there is no induced dipole at all. On the other hand, the dipole moment of y and z components is induced. For the early time, the y component quickly oscillates with the applied field and slowly does as time progresses. The z component is induced largely, which corresponds to easy axis to the polarization owing to the orientation of the molecule with respect to the applied field. Along the z axis the electron can move from lower H atoms to upper H atoms through Si so that the polarization along the z axis becomes large in comparison with that along the y axis. The total dipole moment oscillates and dumpens slowly. Note here that we neglected effects of nuclear motions. If the nuclear motions are treated explicitly, damping behavior is more remarkable.[143] These effects will be treated elsewhere.

In order to detect the electronic motion more precisely, we observed the atom-centered current and atom-centered dipole moment as depicted in Figures 11 and 12. The x component of

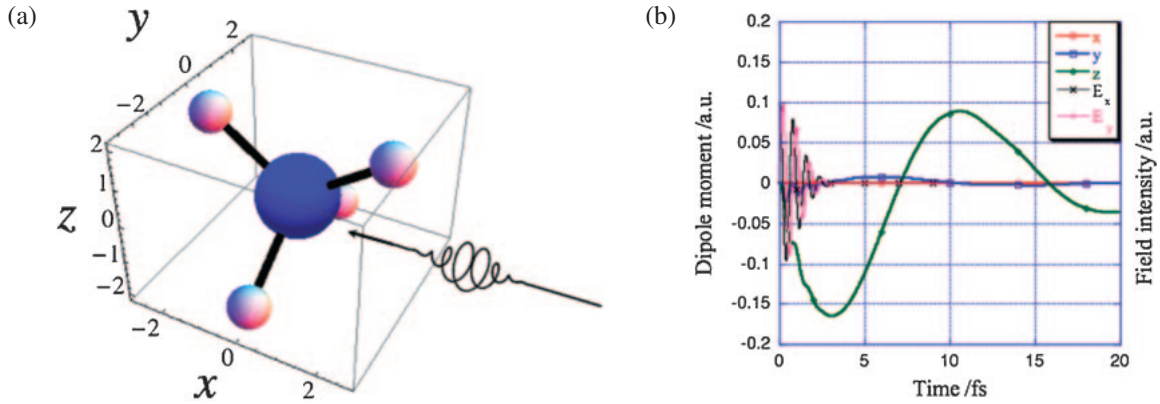

Figure 10. (a) Model system and applied circularly polarized field and (b) intensity of polarized laser field and total induced dipole moment.

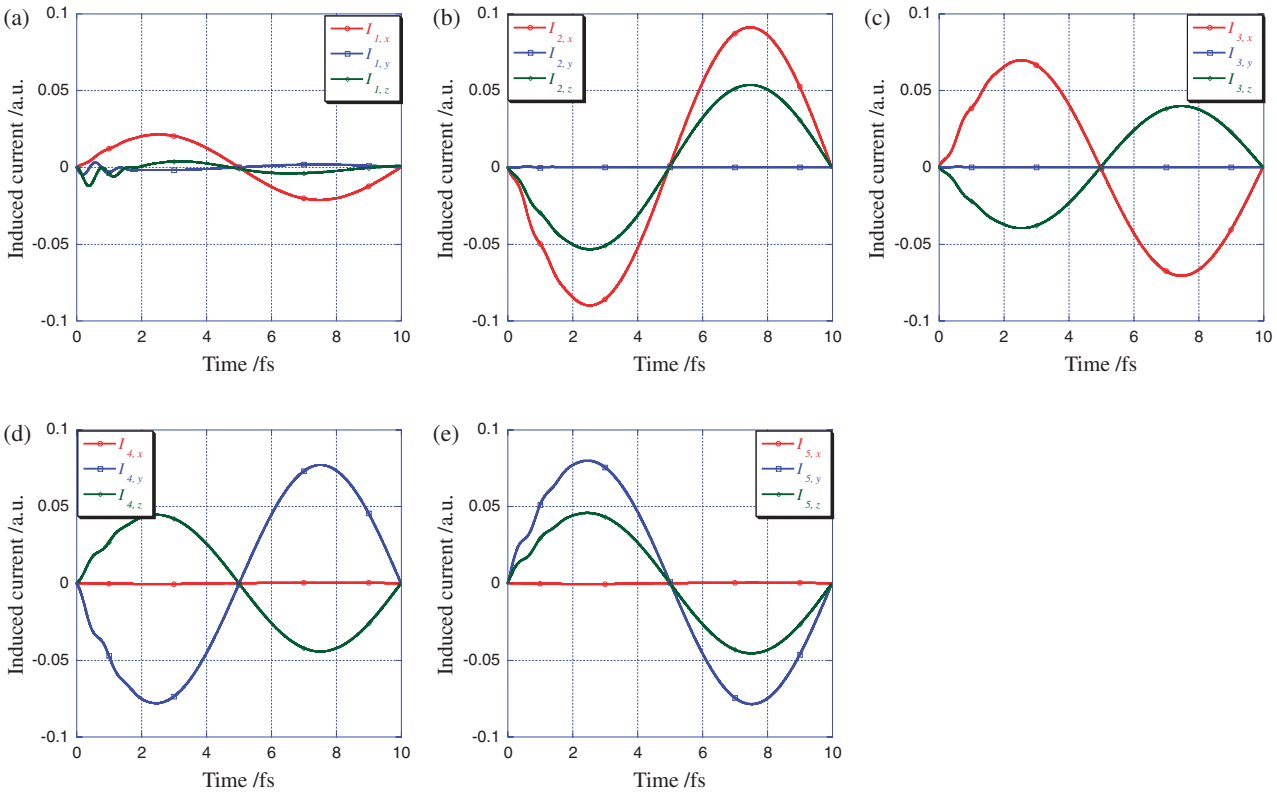

Figure 11. Atom-centered induced current of (a) Si and (b–d) H atoms.

the all atom-centered induced currents is small, but not 0, while y and z components largely oscillate with time. It is found the oscillation with an immediate response to the laser is clearly found at that of the Si atom. Since the polarization of the H atoms is larger than that of the Si atom, such response is buried in the large oscillation. The atom-centered dipole moments oscillate with time but not so remarkable in comparison with the total and the atom-centered currents.

In conclusion of the present section, we have explained RSTDDFT and applied the method to two problems. One is to solve NBO problems by means of an imaginary time evolution operator and the other is to solve the electron dynamics driven by a laser. We confirmed that the methodology could be also applied to NBO problems. For the latter problems, the atom-centered dipole moment and induced current were measured to detect the electronic motion in a molecule.

5. General Conclusion

In this review, we explain recent advances in our theoretical developments and applications to treat thermal fluctuations and quantum effects. In order to treat thermal fluctuation we developed a QM/MM approach. This method is applied to simulate an endohedral fullerene in a crystalline phase. Especially, we performed QM/MM MD simulations of $(Be + nH_2)C_{60}$ ($n = 1$ and 2) and observed the gigantic effective charge fluctuation on the Be atom for $n = 2$. This thermal fluctuation is quite sensitive to the applied temperature and the number of co-encapsulated H_2 molecules. It was

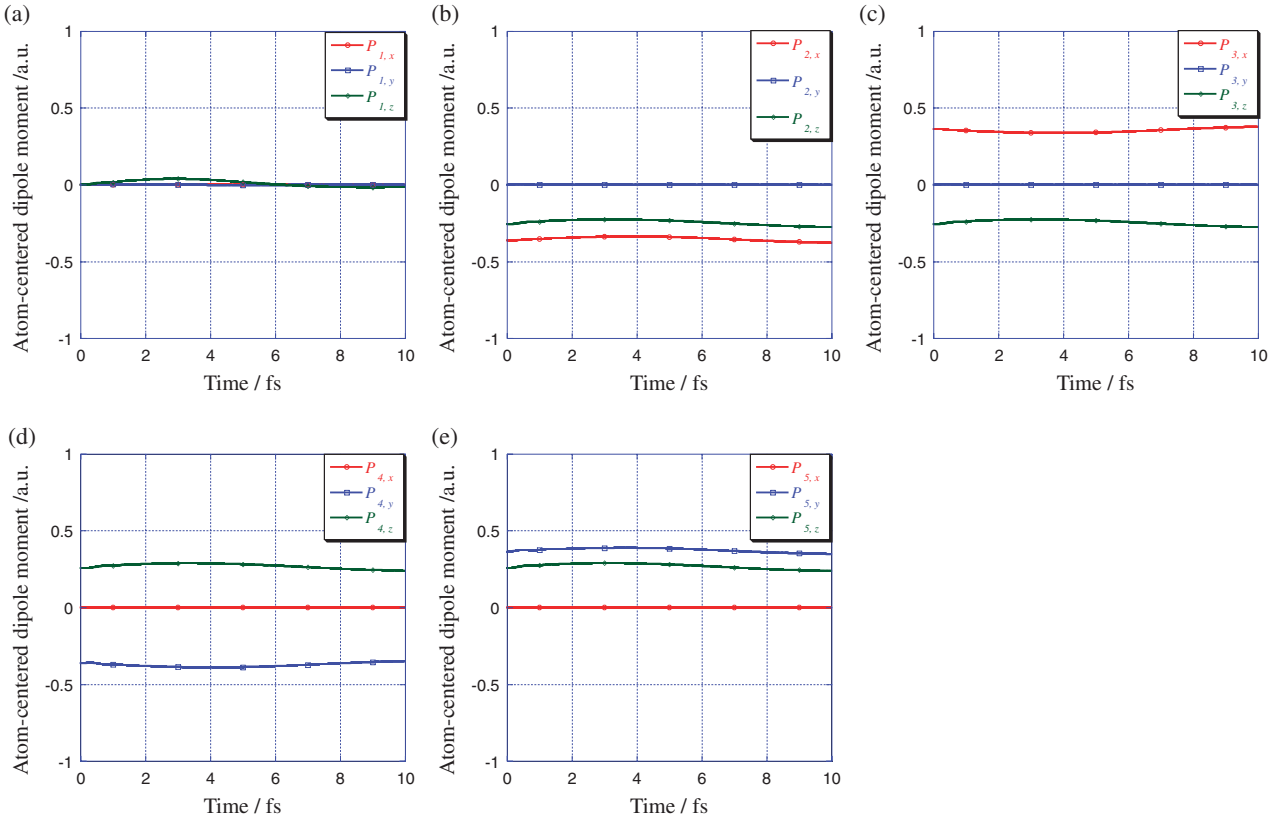

Figure 12. Atom-centered dipole moment of (a) Si and (b–d) H atoms.

found that the fluctuation of the charge on Be has positive correlation with the Be position from the center of the cage. We also investigated the electronic structure in order to specify the reason why the behavior is observed. We clarify that specific molecular orbitals and the polarization due to mixing of 2p orbitals are sensitive to the distance from the center.

We also develop a NBO molecular theory in order to treat the electron and nuclei on equal footings. This method is applied to obtain the electron density and bond lengths of the protonatable amino acid. The results include the nuclear quantum effects so that both the electron density and the bond lengths are vibrationally coupled. It is found that the quantum effects on the electron density are remarkable not only around the position of the hydrogen but also all over the molecule and that the quantum effects elongate the C–H and N–H bonds by about 2%.

The QCD method is developed from the Heisenberg EOM. The methodology is utilized to extend ordinary NMA. We demonstrate that the present method is superior to the typical one in that the present method can describe the inexistence of the vibrational state when a given potential is not shallow enough to allow a vibrational state. The QCD simulation is performed to obtain the vibrational frequencies of small molecules. The results are superior to those obtained by classical dynamics.

The RSTDDFT is implemented and applied to solve the NBO problems and simulate the field-driven electron dynamics. We checked that the NBO problems are solved by applying the imaginary time operator to the given state to yield ground state. The off resonant circularly polarized laser plus is applied to induce electronic fluctuation in a molecule. We measured induced electronic motion by detecting atom centered dipole moment and induced current even by applying the off-resonant laser.

Through the review we emphasized the importance of the thermal fluctuations and quantum effects even in relatively small systems. Thermal fluctuation will be the most important topic in mesoscopic sciences, since the degrees of freedom become numerous so transition from one state to another will often occur. Problems of biological molecules are typical cases. The quantum effects are still hot topics in both molecular and condensed matter sciences, since interests in the both fields overlap with recent advances in nanotechnology. Recently we found unconventional slow electron tunneling occurring at the interface between Si layers (two-dimensional electron gas) and Si grains in SiO_2 (quantum dot). The electronic fluctuation at the two-dimensional electron gas state plays a relevant role in the injection of electrons from the Si layer to the Si dots. Electron dynamics has also solved problems with the development of attosecond laser technology.

The next interesting theme beyond fluctuation we suppose is flow, stream, or current, which is change or transition of a state to anothers. This field has not been studied so deeply yet due to its complexity. Indeed, in biological systems induced excess energy due to chemical reactions is transduced to vibrational motions, driving forces to proceed to other reactions to retransduce the excess energy to chemical energy. Mechanisms of the energy flow from a hot spot to another are still open problems and many are trying to understand at present. We are

also trying to understand the mechanism of proton flow at the entrance of proton pump pathways. We found that the entrance serves as both a collecting site proton and valve to regulate movement of the proton. To further study the flow and fluctuation, both quantum and statistical mechanics should be refined, since the problems are intrinsically non-equilibrium and nonlinear. It is expected that the basics will be further advanced in near future.

This research was supported by the Core Research for Evolutional Science and Technology (CREST) Program "High Performance Computing for Multi-Scale and Multi-Physics Phenomena" of the Japan Science and Technology Agency (JST) and by a Grant-in-Aid for the scientific research on priority area "Molecular theory for real systems" (No. 20038008), and Grant-in-Aid for Young Scientists (B) (No. 20750004).

References

1 I. Prigogine, *The End of Certainty*, The Free Press, NY, **1997**.
2 I. Prigogine, D. Kondepudi, *Themodynamique*, Editions Odile Jacob, Paris, **1999**; Translated in Japanase: M. Imoo, K. Iwamoto, Asakura Press, Tokyo, **2001**.
3 L. D. Landau, E. M. Lifshitz, *Statisitical Physics*, Course of Theoretical Physics, 3rd ed., Butterworth-Heinemann, **1980**, Vol. 5.
4 J. J. Sakurai, *Modern Quantum Mechanics*, Addison Wesley, **1993**.
5 A. L. Fetter, J. D. Walecka, *Quantum Theory of Many-Particle Systems*, Dover Publications, **2003**.
6 G. D. Mahan, *Many-Particle Physics*, 3rd ed., Springer, **2007**.
7 S. Okazaki, *Basic Course of Computer Simulation*, Kagaku-dojin, **2000**.
8 J. C. Tully, *Annu. Rev. Phys. Chem.* **2000**, *51*, 153.
9 W. H. Miller, *J. Phys. Chem. A* **2001**, *105*, 2942.
10 G. A. Fiete, E. J. Heller, *Rev. Mod. Phys.* **2003**, *75*, 933.
11 J. Gao, D. G. Truhlar, *Annu. Rev. Phys. Chem.* **2002**, *53*, 467.
12 M. F. Herman, E. Kluk, *Chem. Phys.* **1984**, *91*, 27.
13 K. G. Kay, *Phys. Rev. A* **1992**, *46*, 1213.
14 G. D. Billing, *Phys. Chem. Chem. Phys.* **2002**, *4*, 2865.
15 C. L. Lopreore, R. E. Wyatt, *Phys. Rev. Lett.* **1999**, *82*, 5190.
16 R. P. Feynman, A. R. Hibbs, *Quantum Mechanics and Path Integrals*, McGraw-Hill, New York, **1965**.
17 R. P. Feynman, H. Kleinert, *Phys. Rev. A* **1986**, *34*, 5080.
18 R. Jackiw, A. Kerman, *Phys. Lett. A* **1979**, *71*, 158.
19 K. Cooper, S.-Y. Pi, P. N. Stancioff, *Phys. Rev. D* **1986**, *34*, 3831.
20 Y. Tsue, Y. Fujiwara, *Prog. Theor. Phys.* **1991**, *86*, 443.
21 Y. Tsue, *Prog. Theor. Phys.* **1992**, *88*, 911.
22 Y. Shigeta, Y. Ozaki, K. Kodama, H. Nagao, H. Kawabe, K. Nishikawa, *Int. J. Quantum Chem.* **1998**, *69*, 629.
23 Y. Shigeta, H. Takahashi, S. Yamanaka, M. Mitani, H. Nagao, K. Yamaguchi, *Int. J. Quantum Chem.* **1998**, *70*, 659.
24 Y. Shigeta, H. Nagao, K. Nishikawa, K. Yamaguchi, *J. Chem. Phys.* **1999**, *111*, 6171; Y. Shigeta, H. Nagao, K. Nishikawa, K. Yamaguchi, *Int. J. Quantum Chem.* **1999**, *75*, 875.
25 H. Nakai, K. Sodeyama, M. Hoshino, *Chem. Phys. Lett.* **2001**, *345*, 118.
26 H. Nakai, *Int. J. Quantum Chem.* **2002**, *86*, 511.
27 H. Nakai, K. Sodeyama, *J. Chem. Phys.* **2003**, *118*, 1119.
28 H. Nakai, M. Hoshino, K. Miyamoto, S. Hyodo, *J. Chem. Phys.* **2005**, *122*, 164101; H. Nakai, M. Hoshino, K. Miyamoto, S. Hyodo, *J. Chem. Phys.* **2005**, *123*, 237102.
29 K. Sodeyama, K. Miyamoto, H. Nakai, *Chem. Phys. Lett.* **2006**, *421*, 72.
30 M. Hoshino, H. Nakai, *J. Chem. Phys.* **2006**, *124*, 194110.
31 K. Miyamoto, M. Hoshino, H. Nakai, *J. Chem. Theory Comput.* **2006**, *2*, 1544.
32 K. Sodeyama, H. Nishizawa, M. Hoshino, M. Kobayashi, H. Nakai, *Chem. Phys. Lett.* **2007**, *433*, 409.
33 Y. Imamura, H. Kiryu, H. Nakai, *J. Comput. Chem.* **2008**, *29*, 735.
34 M. Tachikawa, K. Mori, H. Nakai, K. Iguchi, *Chem. Phys. Lett.* **1998**, *290*, 437.
35 M. Tachikawa, *Chem. Phys. Lett.* **2002**, *360*, 494.
36 T. Ishimoto, M. Tachikawa, M. Yamauchi, H. Kitagawa, H. Tokiwa, U. Nagashima, *Chem. Phys. Lett.* **2003**, *372*, 503; T. Ishimoto, M. Tachikawa, M. Yamauchi, H. Kitagawa, H. Tokiwa, U. Nagashima, *J. Phys. Soc. Jpn.* **2004**, *73*, 1775.
37 T. Ishimoto, M. Tachikawa, H. Tokiwa, U. Nagashima, *Chem. Phys.* **2005**, *314*, 231; T. Ishimoto, M. Tachikawa, H. Tokiwa, U. Nagashima, *J. Phys. Soc. Jpn.* **2005**, *74*, 3112.
38 T. Ishimoto, M. Tachikawa, U. Nagashima, *J. Chem. Phys.* **2006**, *124*, 014112; T. Ishimoto, M. Tachikawa, U. Nagashima, *Int. J. Quantum Chem.* **2006**, *106*, 1465; T. Ishimoto, M. Tachikawa, U. Nagashima, *J. Chem. Phys.* **2006**, *125*, 144103.
39 T. Udagawa, M. Tachikawa, *J. Chem. Phys.* **2006**, *125*, 244105.
40 Y. Itou, S. Mori, T. Udagawa, M. Tachikawa, T. Ishimoto, U. Nagashima, *J. Phys. Chem. A* **2007**, *111*, 261.
41 M. Tachikawa, *J. Phys.: Condens. Matter* **2007**, *19*, 365235.
42 T. Ishimoto, M. Tachikawa, U. Nagashima, *J. Chem. Phys.* **2008**, *128*, 164118.
43 M. Tachikawa, *Integr. Ferroelectr.* **2008**, *100*, 72.
44 T. Iordanov, S. Hammes-Schiffer, *J. Chem. Phys.* **2003**, *118*, 9489.
45 M. V. Pak, C. Swalina, S. P Webb, S. Hammes-Schiffer, *Chem. Phys.* **2004**, *304*, 227.
46 M. V. Pak, S. Hammes-Schiffer, *Phys. Rev. Lett.* **2004**, *92*, 103002.
47 C. Swalina, M. V. Pak, S. Hammes-Schiffer, *Chem. Phys. Lett.* **2005**, *404*, 394.
48 C. Swalina, M. V. Pak, S. Hammes-Schiffer, *J. Chem. Phys.* **2005**, *123*, 014303.
49 A. Reyes, M. V. Pak, S. Hammes-Schiffer, *J. Chem. Phys.* **2005**, *123*, 064104.
50 J. H. Skone, M. V. Pak, S. Hammes-Schiffer, *J. Chem. Phys.* **2005**, *123*, 134108.
51 C. Swalina, M. V. Pak, A. Chakraborty, S. Hammes-Schiffer, *J. Phys. Chem. A* **2006**, *110*, 9983.
52 M. V. Pak, A. Chakraborty, S. Hammes-Schiffer, *J. Phys. Chem. A* **2007**, *111*, 4522.
53 A. Chakraborty, S. Hammes-Schiffer, *J. Chem. Phys.* **2008**, *129*, 204101.
54 A. Chakraborty, M. V. Pak, S. Hammes-Schiffer, *Phys. Rev. Lett.* **2008**, *101*, 153001.
55 A. Hazra, J. H. Skone, S. Hammes-Schiffer, *J. Chem. Phys.*

2009, *130*, 054108.
56 M. V. Pak, A. Chakraborty, S. Hammes-Schiffer, *J. Phys. Chem. A* **2009**, *113*, 4004.
57 O. V. Prezhdo, Y. V. Pereverzev, *J. Chem. Phys.* **2000**, *113*, 6557; O. V. Prezhdo, Y. V. Pereverzev, *J. Chem. Phys.* **2002**, *116*, 4450.
58 E. Pahl, O. V. Prezhdo, *J. Chem. Phys.* **2002**, *116*, 8704.
59 O. V. Prezhdo, *J. Chem. Phys.* **2002**, *117*, 2995.
60 E. Heatwole, O. V. Prezhdo, *J. Chem. Phys.* **2004**, *121*, 10967; E. Heatwole, O. V. Prezhdo, *J. Chem. Phys.* **2005**, *122*, 234109; E. Heatwole, O. V. Prezhdo, *J. Chem. Phys.* **2007**, *126*, 204108.
61 O. V. Prezhdo, *Theor. Chem. Acc.* **2006**, *116*, 206.
62 H. Miyachi, Y. Shigeta, K. Hirao, *Chem. Phys. Lett.* **2006**, *432*, 585.
63 Y. Shigeta, H. Miyachi, K. Hirao, *J. Chem. Phys.* **2006**, *125*, 244102.
64 Y. Shigeta, H. Miyachi, K. Hirao, *Chem. Phys. Lett.* **2007**, *443*, 414.
65 Y. Shigeta, H. Miyachi, T. Matsui, K. Hirao, *Bull. Chem. Soc. Jpn.* **2008**, *81*, 1230.
66 Y. Shigeta, *J. Chem. Phys.* **2008**, *128*, 161103.
67 Y. V. Pereverzev, A. Pereverzev, Y. Shigeta, O. V. Prezhdo, *J. Chem. Phys.* **2008**, *129*, 144104.
68 Y. Shigeta, H. Miyachi, T. Matsui, K. Hirao, in *Advances in the Theory of Atomic and Molecular Systems: Dynamics, Spectroscopy, Clusters, and Nanostructures*, ed. by P. Piecuch, J. Maruani, G. Delgado-Barrio, Springer, **2009**, in press.
69 I. Barth, J. Manz, Y. Shigeta, K. Yagi, *J. Am. Chem. Soc.* **2006**, *128*, 7043.
70 Y. Shigeta, H. Saito, *Synth. Met.* **2003**, *135–136*, 765.
71 Y. Shigeta, *AIP Conf. Proc.* **2004**, *708*, 464.
72 Y. Shigeta, K. Takatsuka, *J. Chem. Phys.* **2005**, *123*, 131101.
73 H. W. Kroto, J. R. Heath, S. C. O'Brien, R. F. Curl, R. E. Smalley, *Nature* **1985**, *318*, 162.
74 W. Krätschmer, L. D. Lamb, K. Fostiropoulos, D. R. Huffman, *Nature* **1990**, *347*, 354.
75 Y. Chai, T. Guo, C. Jin, R. E. Haufler, L. P. F. Chibante, J. Fure, L. Wang, J. M. Alford, R. E. Smalley, *J. Chem. Phys.* **1991**, *95*, 7564.
76 T. Akasaka, S. Nagase, K. Kobayashi, M. Wälchli, K. Yamamoto, H. Funasaka, M. Kako, T. Hoshino, T. Erata, *Angew. Chem., Int. Ed. Engl.* **1997**, *36*, 1643.
77 J. Laskin, T. Peres, C. Lifshitz, M. Snunders, R. J. Cross, A. Khong, *Chem. Phys. Lett.* **1998**, *285*, 7.
78 T. Almeida Murphy, Th. Pawlik, A. Weidinger, M. Höhne, R. Alcala, J.-M. Spaeth, *Phys. Rev. Lett.* **1996**, *77*, 1075.
79 J. Lu, X. Zhang, X. Zhao, *Chem. Phys. Lett.* **1999**, *312*, 85.
80 Y. Murata, M. Murata, K. Komatsu, *J. Am. Chem. Soc.* **2003**, *125*, 7152.
81 K. Komatsu, M. Murata, Y. Murata, *Science* **2005**, *307*, 238.
82 T. Ohtsuki, K. Masumoto, K. Ohno, Y. Maruyama, Y. Kawazoe, K. Sueki, K. Kikuchi, *Phys. Rev. Lett.* **1996**, *77*, 3522; T. Ohtsuki, H. Yuki, M. Muto, J. Kasagi, K. Ohno, *Phys. Rev. Lett.* **2004**, *93*, 112501.
83 L. Türker, *THEOCHEM* **2002**, *577*, 205.
84 Y. Shigeta, *Int. J. Quantum Chem.* **2004**, *96*, 32.
85 M. J. Field, P. A. Bash, M. J. Karplus, *J. Comput. Chem.* **1990**, *11*, 700.
86 A. K. Rappé, W. A. Goddard, III, *J. Phys. Chem.* **1991**, *95*, 3358.
87 M. J. Frisch, G. W. Trucks, H. B. Schlegel, G. E. Scuseria, M. A. Robb, J. R. Cheeseman, V. G. Zakrzewski, J. A. Montgomery, Jr., R. E. Stratmann, J. C. Burant, S. Dapprich, J. M. Millam, A. D. Daniels, K. N. Kudin, M. C. Strain, O. Farkas, J. Tomasi, V. Barone, M. Cossi, R. Cammi, B. Mennucci, C. Pomelli, C. Adamo, S. Clifford, J. Ochterski, G. A. Petersson, P. Y. Ayala, Q. Cui, K. Morokuma, D. K. Malick, A. D. Rabuck, K. Raghavachari, J. B. Foresman, J. Cioslowski, J. V. Ortiz, B. B. Stefanov, G. Liu, A. Liashenko, P. Piskorz, I. Komaromi, R. Gomperts, R. L. Martin, D. J. Fox, T. Keith, M. A. Al-Laham, C. Y. Peng, A. Nanayakkara, C. Gonzalez, M. Challacombe, P. M. W. Gill, B. Johnson, W. Chen, M. W. Wong, J. L. Andres, C. Gonzalez, M. Head-Gordon, E. S. Replogle, J. A. Pople, *Gaussian 98, Revision A6*, Gaussian Inc., Pittsburgh PA, **1998**; M. J. Frisch, G. W. Trucks, H. B. Schlegel, G. E. Scuseria, M. A. Robb, J. R. Cheeseman, J. A. Montgomery, Jr., T. Vreven, K. N. Kudin, J. C. Burant, J. M. Millam, S. S. Iyengar, J. Tomasi, V. Barone, B. Mennucci, M. Cossi, G. Scalmani, N. Rega, G. A. Petersson, H. Nakatsuji, M. Hada, M. Ehara, K. Toyota, R. Fukuda, J. Hasegawa, M. Ishida, T. Nakajima, Y. Honda, O. Kitao, H. Nakai, M. Klene, X. Li, J. E. Knox, H. P. Hratchian, J. B. Cross, C. Adamo, J. Jaramillo, R. Gomperts, R. E. Stratmann, O. Yazyev, A. J. Austin, R. Cammi, C. Pomelli, J. W. Ochterski, P. Y. Ayala, K. Morokuma, G. A. Voth, P. Salvador, J. J. Dannenberg, V. G. Zakrzewski, S. Dapprich, A. D. Daniels, M. C. Strain, O. Farkas, D. K. Malick, A. D. Rabuck, K. Raghavachari, J. B. Foresman, J. V. Ortiz, Q. Cui, A. G. Baboul, S. Clifford, J. Cioslowski, B. B. Stefanov, G. Liu, A. Liashenko, P. Piskorz, I. Komaromi, R. L. Martin, D. J. Fox, T. Keith, M. A. Al-Laham, C. Y. Peng, A. Nanayakkara, M. Challacombe, P. M. W. Gill, B. Johnson, W. Chen, M. W. Wong, C. Gonzalez, J. A. Pople, *Gaussian 03, Revision E.01*, Gaussian Inc., Pittsburgh PA, **2003**.
88 M. J. S. Dewar, E. G. Zoebisch, E. F. Healy, J. J. P. Stewart, *J. Am. Chem. Soc.* **1985**, *107*, 3902.
89 M. W. Schmidt, K. K. Baldridge, J. A. Boatz, S. T. Elbert, M. S. Gordon, J. H. Jensen, S. Koseki, N. Matsunaga, K. A. Nguyen, S. Su, T. L. Windus, M. Dupuis, J. A. Montgomery, *J. Comput. Chem.* **1993**, *14*, 1347.
90 S. Nosé, *Prog. Theor. Phys. Suppl.* **1991**, *103*, 1.
91 J. H. Lii, N. L. Allinger, *J. Am. Chem. Soc.* **1989**, *111*, 8576.
92 I. L. Thomas, *Phys. Rev.* **1969**, *185*, 90.
93 J. E. Mayer, *J. Chem. Phys.* **1937**, *5*, 67.
94 R. Kubo, *J. Phys. Soc. Jpn.* **1962**, *17*, 1100.
95 F. Colmenero, C. P. del Valle, C. Valdemoro, *Phys. Rev. A* **1993**, *47*, 971; F. Colmenero, C. P. del Valle, C. Valdemoro, *Phys. Rev. A* **1993**, *47*, 979.
96 D. A. Mazziotti, *Chem. Phys. Lett.* **1998**, *289*, 419.
97 T. Yanai, G. K.-L. Chan, *J. Chem. Phys.* **2006**, *124*, 194106.
98 S. H. Mandal, G. Sanyal, D. Mukherjee, *Lect. Notes Phys.* **1998**, *510*, 93.
99 P. Hohenberg, W. Kohn, *Phys. Rev.* **1964**, *136*, B864.
100 W. Kohn, L. J. Sham, *Phys. Rev.* **1965**, *140*, A1133.
101 R. O. Jones, O. Gunnarsson, *Rev. Mod. Phys.* **1989**, *61*, 689.
102 J. F. Capitani, R. F. Nalewajski, R. G. Parr, *J. Chem. Phys.* **1982**, *76*, 568.
103 E. S. Kryachko, E. V. Ludena, V. Mujica, *Int. J. Quantum Chem.* **1991**, *40*, 589.
104 N. Gidopoulos, *Phys. Rev. B* **1998**, *57*, 2146.

105 J. Drenth, *Principles of Protein X-Ray Crystallography*, Springer, **2003**.
106 T. Chatake, A. Osterman, K. Kurihara, F. G. Parak, N. Niimura, *Proteins* **2003**, *50*, 516.
107 T. Sako, K. Yamanouchi, *Chem. Phys. Lett.* **1997**, *264*, 403.
108 T. Sako, A. Hishikawa, K. Yamanouchi, *Chem. Phys. Lett.* **1998**, *294*, 571.
109 M. Aida, M. Dupuis, *THEOCHEM* **2003**, *633*, 247.
110 M. Aida, M. Dupuis, *Chem. Phys. Lett.* **2005**, *401*, 170.
111 P. A. Frantsuzov, D. Meluzzi, V. A. Mandelshtam, *Phys. Rev. Lett.* **2006**, *96*, 113401.
112 K. Yagi, G. V. Mil'nikov, T. Taketsugu, K. Hirao, H. Nakamura, *Chem. Phys. Lett.* **2004**, *397*, 435.
113 K. Yagi, K. Hirao, T. Taketsugu, M. W. Schmidt, M. S. Gordon, *J. Chem. Phys.* **2004**, *121*, 1383.
114 C. Møller, M. S. Plesset, *Phys. Rev.* **1934**, *46*, 618.
115 R. A. Kendall, T. H. Dunning, Jr., R. J. Harrison, *J. Chem. Phys.* **1992**, *96*, 6796.
116 H. Nagao, K. Kodama, Y. Shigeta, H. Kawabe, K. Nishikawa, M. Nakano, K. Yamaguchi, *Int. J. Quantum Chem.* **1996**, *60*, 1261.
117 H. Nagao, M. Nakano, S. Yamanaka, S. Yamada, D. Yamaki, I. Shigemoto, S. Kiribayashi, K. Yamaguchi, Y. Shigeta, *Int. J. Quantum Chem.* **1996**, *60*, 1291.
118 H. Takahashi, T. Hori, H. Hashimoto, T. Nitta, *J. Comput. Chem.* **2001**, *22*, 1252.
119 H. Takahashi, S. Takei, T. Hori, T. Nitta, *THEOCHEM* **2003**, *632*, 185.
120 H. Takahashi, H. Hashimoto, T. Nitta, *J. Chem. Phys.* **2003**, *119*, 7964.
121 T. Hori, H. Takahashi, T. Nitta, *J. Chem. Phys.* **2003**, *119*, 8492.
122 S. Goedecker, *Rev. Mod. Phys.* **1999**, *71*, 1085.
123 J. R. Chelikowsky, N. Troullier, K. Wu, Y. Saad, *Phys. Rev. B* **1994**, *50*, 11355.
124 J. R. Chelikowsky, *J. Phys. D: Appl. Phys.* **2000**, *33*, R33.
125 T. Hoshi, M. Arai, T. Fujiwara, *Phys. Rev. B* **1995**, *52*, R5459.
126 K. Yabana, G. F. Bertsch, *Phys. Rev. B* **1996**, *54*, 4484.
127 E. L. Briggs, D. J. Sullivan, J. Bernholc, *Phys. Rev. B* **1996**, *54*, 14362.
128 T. L. Beck, *Rev. Mod. Phys.* **2000**, *72*, 1041.
129 K. Hirose, T. Ono, Y. Fujimoto, S. Tsukamoto, *First-Principles Calculation in Real-Space Formalism, Electronic Configurations and Transport Properties of Nanostructures*, Imperial College Press, London, **2005**.
130 J.-I. Iwata, K. Shiraishi, A. Oshiyama, *Phys. Rev. B* **2008**, *77*, 115208.
131 T. Yanai, G. I. Fann, Z. Gan, R. J. Hurrison, G. Beylkin, *J. Chem. Phys.* **2004**, *121*, 6680.
132 T. Shiozaki, S. Hirata, *Phys. Rev. A* **2007**, *76*, 040503.
133 J. P. Perdew, A. Zunger, *Phys. Rev. B* **1981**, *23*, 5048.
134 N. Troullier, J. L. Martins, *Phys. Rev. B* **1991**, *43*, 1993.
135 L. Kleinman, D. M. Bylander, *Phys. Rev. Lett.* **1982**, *48*, 1425.
136 D. B. Kinghorn, L. Adamowicz, *J. Chem. Phys.* **2000**, *113*, 4203.
137 L. D. Noordam, R. R. Jones, *J. Mod. Opt.* **1997**, *44*, 2515.
138 T. C. Weinacht, J. Ahn, P. H. Bucksbaum, *Phys. Rev. Lett.* **1998**, *80*, 5508.
139 T. C. Weinacht, J. Ahn, P. H. Bucksbaum, *Nature* **1999**, *397*, 233.
140 H. Maeda, D. V. L. Norum, T. F. Gallagher, *Science* **2005**, *307*, 1757.
141 K. Hoki, D. Kröner, J. Manz, *J. Chem. Phys.* **2001**, *267*, 59.
142 K. Hoki, M. Yamaki, S. Koseki, Y. Fujimura, *J. Chem. Phys.* **2003**, *118*, 497.
143 M. Kanno, H. Kono, Y. Fujimura, *Angew. Chem., Int. Ed.* **2006**, *45*, 7995.
144 M. Kanno, K. Hoki, H. Kono, Y. Fujimura, *J. Chem. Phys.* **2007**, *127*, 204314.

Yasuteru Shigeta received his diploma in 1995 from Kanazawa University, Japan, and D.Sc. in 2000 from Osaka University, Japan. After a Japan Society for the Promotion of Science postdoctoral fellowship at the Graduate School of Arts and Sciences, The University of Tokyo, He served as Assistant Professor in the Applied Chemistry Department at The University of Tokyo. Following research at University of Tsukuba as a Lecturer (2007–2008), he became an Associate Professor in the Picobiology Institute at the University of Hyogo (2008–present). He received the PCCP Prize for Outstanding Achievement of Young Scientists in Physical Chemistry and Chemical Physics in 2007. His research activities cover the field of chemical physics, including ab initio quantum chemistry and molecular dynamics as well as theoretical nano- and biomaterials. In particular he has developed novel methodology to treat nuclear quantum effects. Recently his research directions are (1) electron dynamics in molecules, metalloproteins, and at the interface between 2-dimensional electron gas and quantum dots, (2) proton-coupled electron transfer in biomolecules, (3) nanomaterials that consists of DNA and artificial DNA, and (4) proton pumping mechanisms in proteins by using electronic structure theory and first principle molecular dynamics.